

Northumbria Research Link

Citation: Stylianidis, Nearchos, Azimov, Ulugbek, Maheri, Alireza, Tomita, Eiji and Kawahara, Nobuyuki (2017) Chemical kinetics and CFD analysis of supercharged micro-pilot ignited dual-fuel engine combustion of syngas. *Fuel*, 203. pp. 591-606. ISSN 0016-2361

Published by: Elsevier

URL: <https://doi.org/10.1016/j.fuel.2017.04.125> <<https://doi.org/10.1016/j.fuel.2017.04.125>>

This version was downloaded from Northumbria Research Link:
<http://nrl.northumbria.ac.uk/30902/>

Northumbria University has developed Northumbria Research Link (NRL) to enable users to access the University's research output. Copyright © and moral rights for items on NRL are retained by the individual author(s) and/or other copyright owners. Single copies of full items can be reproduced, displayed or performed, and given to third parties in any format or medium for personal research or study, educational, or not-for-profit purposes without prior permission or charge, provided the authors, title and full bibliographic details are given, as well as a hyperlink and/or URL to the original metadata page. The content must not be changed in any way. Full items must not be sold commercially in any format or medium without formal permission of the copyright holder. The full policy is available online: <http://nrl.northumbria.ac.uk/policies.html>

This document may differ from the final, published version of the research and has been made available online in accordance with publisher policies. To read and/or cite from the published version of the research, please visit the publisher's website (a subscription may be required.)

www.northumbria.ac.uk/nrl



Manuscript Number: JFUE-D-16-01365R1

Title: Chemical kinetics and CFD analysis of supercharged micro-pilot ignited dual-fuel engine combustion of syngas

Article Type: Research paper

Keywords: Dual-fuel engine, Syngas combustion, Chemical kinetics, DARS, CFD simulation

Corresponding Author: Dr. Ulugbek Azimov, PhD

Corresponding Author's Institution: University of Northumbria

First Author: Nearchos Stylianidis

Order of Authors: Nearchos Stylianidis; Ulugbek Azimov, PhD; Alireza Maheri, PhD; Nobuyuki Kawahara; Eiji Tomita

Abstract: A comprehensive chemical kinetics and computational fluid-dynamics (CFD) analysis were performed to evaluate the combustion of syngas derived from biomass and coke-oven solid feedstock in a micro-pilot ignited supercharged dual-fuel engine under lean conditions. The developed syngas chemical kinetics mechanism was validated by comparing ignition delay, in-cylinder pressure, temperature and laminar flame speed predictions against corresponding experimental and simulated data obtained by using the most commonly used chemical kinetics mechanisms developed by other authors. Sensitivity analysis showed that reactivity of syngas mixtures was found to be governed by H₂ and CO chemistry for hydrogen concentrations lower than 50% and mostly by H₂ chemistry for hydrogen concentrations higher than 50%. In the mechanism validation, particular emphasis is placed on predicting the combustion under high pressure conditions. For high hydrogen concentration in syngas under high pressure, the reactions $\text{HO}_2 + \text{HO}_2 = \text{H}_2\text{O}_2 + \text{O}_2$ and $\text{H}_2\text{O}_2 + \text{H} = \text{H}_2 + \text{HO}_2$ were found to play important role in in-cylinder combustion and heat production. The rate constants for $\text{H}_2\text{O}_2 + \text{H} = \text{H}_2 + \text{HO}_2$ reaction showed strong sensitivity to high-pressure ignition times and has considerable uncertainty. Developed mechanism was used in CFD analysis to predict in-cylinder combustion of syngas and results were compared with experimental data. Crank angle-resolved spatial distribution of in-cylinder spray and combustion temperature was obtained. The constructed mechanism showed the closest prediction of combustion for both biomass and coke-oven syngas in a micro-pilot ignited supercharged dual-fuel engine.

- CFD-compatible syngas chemical kinetics mechanism has been developed for micro-pilot ignited supercharged dual-fuel engine combustion.
- The new mechanism predicted in-cylinder combustion performance well for both biomass and coke-oven syngas.
- Due to the strong temperature dependence of $\text{HO}_2 + \text{OH} = \text{H}_2\text{O} + \text{O}_2$ reaction, two expressions of this reaction were used to accurately simulate biomass-derived syngas.
- To accurately simulate coke-oven syngas, the rate parameter for $\text{H}_2\text{O}_2 + \text{H} = \text{H}_2 + \text{HO}_2$ reaction had to be adopted from Hong et al.[49] with the adjusted power factor, with the rate which is outside of the uncertainty factor limits proposed by Konnov [42].

1 **Chemical kinetics and CFD analysis of supercharged micro-pilot ignited dual-fuel**
2 **engine combustion of syngas**

3
4 *Nearchos Stylianidis¹, Ulugbek Azimov^{1*}, Alireza Maheri¹, Eiji Tomita², Nobuyuki Kawahara²*

5
6 ¹*Department of Mechanical and Construction Engineering, University of Northumbria, City campus, Newcastle*
7 *upon Tyne, NE1 8ST, United Kingdom*

8 ²*Department of Mechanical Engineering, Okayama University, Tsushima-Naka 3, Okayama 700-8530, Japan*

9
10 *Corresponding author:
11 Dr. Ulugbek Azimov
12 Senior Lecturer
13 Dept. of Mechanical and Construction Engineering
14 University of Northumbria
15 City Campus, Wynne-Jones Centre, Room 305
16 Newcastle upon Tyne
17 NE1 8ST, UK
18 Phone: +44 191-2437663
19 Email: ulugbek.azimov@northumbria.ac.uk

20
21 Dr. Alireza Maheri
22 Senior Lecturer
23 Dept. of Mechanical and Construction Engineering
24 University of Northumbria
25 City Campus, Wynne-Jones Centre, Room 201
26 Newcastle upon Tyne
27 NE1 8ST, UK
28 Phone: +44 191-2433860
29 Email: alireza.maheri@northumbria.ac.uk

30
31 Mr. Nearchos Stylianidis
32 PhD student
33 Dept. of Mechanical and Construction Engineering
34 University of Northumbria
35 City Campus, Wynne-Jones Centre, Room 209
36 Newcastle upon Tyne
37 NE1 8ST, UK
38 Email: nearchos.stylianidis@northumbria.ac.uk

39
40 Prof. Nobuyuki Kawahara
41 Dept. of Mechanical Engineering, Okayama University
42 3-1-1 Tsushima-naka, Kita-ku, Okayama 700-8530, JAPAN
43 Phone: +81-86-251-8235
44 FAX: +81-86-251-8266
45 Email: kawahara@mech.okayama-u.ac.jp

46
47

48 Prof. Eiji Tomita
49 Dept. of Mechanical Engineering, Okayama University
50 3-1-1 Tsushima-naka, Kita-ku, Okayama 700-8530, JAPAN
51 Phone: +81-86-251-8049
52 FAX: +81-86-251-8266
53 Email: tomita@mech.okayama-u.ac.jp

54
55
56

57 **Nomenclature**

58
59 BTDC: Before top dead centre
60 ATDC: After top dead centre
61 CA: Crank angle
62 CI: Compression ignition
63 CNG: Compressed natural gas
64 IC: Internal combustion
65 ROHR (J/deg): Rate of heat release
66 SI: Spark ignition
67 TDC: Top dead centre
68 BMG: Biomass Gasification
69 COG: Coke-Oven Gasification

70
71
72
73
74
75
76
77
78
79
80
81
82
83
84
85
86
87
88
89
90
91
92
93

94 **Chemical kinetics and CFD analysis of supercharged micro-pilot ignited dual-fuel**
95 **engine combustion of syngas**

96
97 *Nearchos Stylianidis¹, Ulugbek Azimov^{1*}, Alireza Maheri¹, Eiji Tomita², Nobuyuki Kawahara²*

98
99 ¹*Department of Mechanical and Construction Engineering, University of Northumbria, City campus, Newcastle*
100 *upon Tyne, NE1 8ST, United Kingdom*

101 ²*Department of Mechanical Engineering, Okayama University, Tsushima-Naka 3, Okayama 700-8530, Japan*

102
103 **Abstract**

104 A comprehensive chemical kinetics and computational fluid-dynamics (CFD) analysis were performed to
105 evaluate the combustion of syngas derived from biomass and coke-oven solid feedstock in a micro-pilot
106 ignited supercharged dual-fuel engine under lean conditions. The developed syngas chemical kinetics
107 mechanism was validated by comparing ignition delay, in-cylinder pressure, temperature and laminar flame
108 speed predictions against corresponding experimental and simulated data obtained by using the most
109 commonly used chemical kinetics mechanisms developed by other authors. Sensitivity analysis showed that
110 reactivity of syngas mixtures was found to be governed by H₂ and CO chemistry for hydrogen concentrations
111 lower than 50% and mostly by H₂ chemistry for hydrogen concentrations higher than 50%. In the mechanism
112 validation, particular emphasis is placed on predicting the combustion under high pressure conditions. For high
113 hydrogen concentration in syngas under high pressure, the reactions HO₂+HO₂=H₂O₂+O₂ and
114 H₂O₂+H=H₂+HO₂ were found to play important role in in-cylinder combustion and heat production. The rate
115 constants for H₂O₂+H=H₂+HO₂ reaction showed strong sensitivity to high-pressure ignition times and has
116 considerable uncertainty. Developed mechanism was used in CFD analysis to predict in-cylinder combustion
117 of syngas and results were compared with experimental data. Crank angle-resolved spatial distribution of
118 in-cylinder spray and combustion temperature was obtained. The constructed mechanism showed the closest
119 prediction of combustion for both biomass and coke-oven syngas in a micro-pilot ignited supercharged
120 dual-fuel engine.

121 **Keywords:** Dual-fuel engine, Syngas combustion, Chemical kinetics, DARS, CFD simulation

122

123 1. Introduction

124 Advanced reciprocating engines are considered a potential means of converting syngas into power because
125 of their role in distributed energy production and their combination of high efficiency and low cost [1]. Syngas
126 consists of combustible gases composed of mainly carbon monoxide (CO), hydrogen (H₂), and methane (CH₄),
127 and non-combustible gases composed of mainly nitrogen (N₂) and carbon dioxide (CO₂). Varying proportions
128 of H₂, CO, CH₄, CO₂, H₂O, and N₂ may be present [2]. Mixtures of H₂ and CO have high antiknock behaviour
129 and therefore could serve as fuels for internal combustion engines [3, 4]. However, the addition of hydrogen to
130 carbon monoxide or methane tends to increase combustion temperatures and NO_x emissions under
131 stoichiometric conditions [5]. Therefore, such mixtures are more appropriate for lean-burn applications, where
132 combustion temperatures are moderated by excess air.

133 The main benefit of utilizing syngas as a fuel for power generation is obtained when syngas is used in
134 dual-fuel engines that operate under compression ignition with a lean mixture, using a pilot injection of diesel
135 fuel [8]. Some fuels do not have sufficient ignition properties to enable ignition, so two fuels must be used. The
136 ignition of the primary fuel (typically gaseous) is activated by the in-cylinder conditions. In this case, first, a
137 pilot diesel fuel is injected, resulting in ignition and a subsequent temperature rise in the combustion
138 chamber [7, 8]. Then, the primary gaseous fuel, which in this case is syngas, is ignited as the chamber
139 temperature increases, with subsequent combustion. Dual-fuel engines have been employed for a wide range of
140 applications to utilize gaseous fuels. They are most commonly modified diesel engines and can achieve very
141 low emission levels, particularly for smoke and particulates. The benefits of the dual-fuel conversion, if
142 compared to the conventional diesel engine operation, include high efficiency, fuel flexibility, smoother and
143 quieter operation, significantly longer engine life between overhauls, fuel savings, and enhanced safety.

144 A few published works have described the use of syngas as a fuel for internal combustion (IC) engines.
145 These include the work of Karim and coworkers [9, 10], McMillian and Lawson [11], Christodoulou and
146 Megaritis [12]. Bilcan [13] studied the use of various gaseous fuels, including syngas, in dual-fuel engines.

147 Baratieri *et al.* [14] conducted a comparative analysis on the use of biomass-based syngas in
148 internal-combustion (IC) engines and combined-cycle gas turbine (CCGT) plants. They concluded that the IC
149 engine configuration is characterized by a significant thermal energy fraction that makes it possible to reach
150 global energy efficiencies higher than 70%. Boehman and Le Corre [15] surveyed the published work on
151 syngas combustion in reciprocating engines and focused on dual-fuel combustion in compression-ignition
152 engines. Tomita *et al.* [16] investigated the combustion characteristics and performance of supercharged
153 syngas with micro-pilot ignition in a dual-fuel engine. With a certain increase in syngas hydrogen content, the
154 engine was found to operate with stable combustion and high efficiency, even at an equivalence ratio of 0.45,
155 because the increased hydrogen content enhanced the lean limit of the mixture. Roy *et al.* [17, 18] studied the
156 effect of hydrogen content in the syngas produced from biomass and the effect of exhaust gas recirculation
157 (EGR) in the syngas produced from hydrogen-rich coke oven gas on the performance and exhaust emissions of
158 a dual-fuel engine. They found that the engine power with the high-H₂-content syngas increased by 12%, and
159 that the high-H₂-content syngas was superior to the low-H₂-content gas for leaner operations.

160 Because the composition of syngas depends on the solid feedstock and its gasification process, it is very
161 difficult to model and predict engine in-cylinder syngas combustion. A universal CFD-compatible syngas
162 chemical kinetics mechanism must be developed that could cover the broad range of syngas composition and
163 engine combustion conditions. While developing syngas mechanism usually H₂/CO structure is considered,
164 however some syngas types derived from biomass and coke-oven solid feedstock may also include CH₄, as
165 shown in this paper. Another complexity rises due to the effect of in-cylinder turbulence on combustion.

166 Improvements made to the fuel flexibility of syngas-combustion technology by optimizing the combustion
167 mechanism will provide for an increased acceptable range in the variation of fuel composition and conditions.
168 Several research groups have developed chemical kinetics mechanisms to simulate syngas combustion.
169 Yetter *et al.* [19] developed a comprehensive reaction mechanism for CO and H₂, which are considered the
170 main combustible species in syngas. Saxena and Williams [20] tested a small detailed chemical kinetic

171 mechanism for the combustion of hydrogen and carbon monoxide. They made a few revisions to the rate
172 parameters for the elementary steps in the mechanism for hydrogen [21–24], deleted the hydrogen initiation
173 step, and added an initiation step for CO along with changes to the three-body recombination rates and
174 chaperon efficiencies. They reported that with these changes, a reasonable agreement was obtained with
175 measured burning velocities, diffusion-flame extinction conditions, and autoignition times. Frassoldati *et al.*
176 [25, 26] studied the combustion and flame structure of CO–H₂ mixtures. They developed a kinetic scheme for
177 turbulent diffusion flames by coupling a kinetic postprocessor with a computational fluid dynamics (CFD)
178 code to investigate the flame structure and pollutant formation. Slavinskaya *et al.* [27] developed a skeletal
179 reaction mechanism for syngas combustion in gas turbines with 12 species and 20 irreversible reactions. This
180 mechanism was validated for pressures up to 20 bar with different mixture contents and fuel–air ratios. Starik
181 *et al.* [28] developed a kinetic model that describes the processes of ignition and combustion of CO–H₂–O₂–N₂
182 mixtures. The model was validated over wide ranges of temperature, pressure, and equivalence ratio using
183 experimental data for the ignition delay time and laminar-flame propagation velocity, and also for the evolution
184 of the most important species. Sun *et al.* [29] studied high-pressure flame speeds and performed kinetic
185 modelling of CO/H₂ combustion. The comparison between the modelled results and laboratory measurements
186 suggested that the accuracy of the thermochemical data and the elementary rate constants is crucial for
187 obtaining satisfactory performance of the reaction mechanism. Sivaramakrishnan *et al.* [30] studied the
188 combustion of CO/H₂ mixtures at elevated pressures. They showed that the model they developed
189 underpredicted CO and O₂ decay and CO₂ formation at very high pressures of 256 and 450 bars. They
190 concluded that HO₂ radical reactions appear to be among the most sensitive reactions in the model under these
191 conditions. Cavaliere *et al.* [31] modelled kinetically the ignition of syngas/air mixtures at low temperature and
192 high pressure with the four reaction mechanisms described by Frassoldati *et al.* [25], Saxena and Williams [20],
193 Yetter *et al.* [19], and GRI Mech 3.0 [32]. They found that for a mixture of CO and H₂, all mechanisms
194 predicted the experimental data accurately for temperatures above 1000 K regardless of the pressure. But

195 below this temperature, the simulation results deviated from the experimental data. Mittal *et al.* [33] used
196 experiments with a rapid-compression machine and numerical studies to evaluate the combustion mechanism
197 for CO/H₂ mixtures at high pressures in the range of 15–50 bar and at temperatures of 950–1100 K. Their
198 results demonstrated that any evaluation of a kinetic scheme by reference to ignition delays must be treated
199 with some caution when the kinetic uncertainties are not taken into account. Chaos and Dryer [34] reviewed
200 the possibility of using gas turbine syngas combustion with higher pressures and lower temperatures to test the
201 comprehensive nature of the existing detailed chemical kinetic models. They proposed kinetic changes to
202 improve the predictions of syngas combustion under these conditions and emphasized that the higher-pressure,
203 lower-temperature conditions encountered in gas turbines point to the importance of and the need for further
204 theoretical as well as experimental studies of elementary reactions involving HO₂ and H₂O₂ chemistry.

205 Keromnes *et al.* [35] performed detailed chemical kinetic modelling study of hydrogen and syngas
206 mixtures at elevated pressures and presented new oxidation data. The mechanism accurately reproduces
207 high-pressure and intermediate- to high-temperature data relevant to gas turbine conditions. They showed that
208 syngas chemistry is governed by the hydrogen chemistry, and CO addition has an inhibiting effect. The
209 predictions of the mechanism for a series of fundamental shock tube, RCM, and flame speed experiments are
210 in good agreement. However, some differences appear at low to intermediate temperatures due to the
211 importance of the oxidation pathway through reactions $\text{H}+\text{O}_2(+\text{M})=\text{HO}_2(+\text{M})$, $\text{H}_2\text{O}_2(+\text{M})=\text{OH}+\text{OH}(+\text{M})$ and
212 $\text{H}_2\text{O}_2+\text{H}=\text{H}_2+\text{HO}_2$.

213 Lee *et al.* [36] performed comprehensive comparison of chemical kinetics mechanisms for syngas/biogas
214 mixtures. They found that NUIG2013 mechanism [37] was in closest agreement with the measured ignition
215 delay and laminar flame speed for the investigated mixtures. However, there are several mixture compositions
216 and conditions for which the NUIG2013 mechanism fails to accurately predict the ignition delay time results.
217 These include syngas mixtures with CH₄ gas content, and CH₄/H₂ mixtures at low hydrogen concentrations
218 ($\leq 40\%$ H₂).

219 Olm et al. [38] compared 16 chemical kinetics mechanisms developed by different authors and identified
220 well performing mechanisms and those that are only good at certain conditions for a certain types of
221 experiments. They have concluded that three of syngas mechanisms, Keromnes-2013 [35], NUIG-NGM-2010
222 [39] and Li-2007 [40] showed closest match with experiments, while others may only excel in certain
223 categories and are not able to provide general reliability across the various types of experiments.

224 The syngas mechanisms described above were mainly developed under the conditions which excluded the
225 effect of turbulence and they are not able to accurately represent the interactions between turbulent fluid
226 dynamics and chemical kinetics in an IC engine cylinder. These turbulence–chemistry interactions can have
227 significant effects on ignition delay, flame stability and pollutant formation during engine combustion. There is
228 an urgent need for a reliable engine-simulation model that represents the turbulence–chemistry interactions by
229 combining CFD and a syngas chemical kinetics. It has been shown that the effects of turbulent mixing must be
230 considered to obtain better agreement with experiments during the combustion phase [41]. In earlier studies we
231 made an attempt to analyse dual-fuel engine combustion with syngas and developed a syngas chemical kinetics
232 mechanism. In this work the important hydrogen-based reaction rates proposed by Keromnes et al. [35] and
233 Konnov [42] were included into mechanism and comprehensive study was performed to develop IC
234 engine-compatible syngas chemical kinetics mechanism and validate against engine experiments. This model
235 will help predict the combustion behaviour of syngas with various chemical compositions from different
236 feedstock, such as biomass, coal, and refinery residues, as a necessary precondition for establishing numerical
237 tools to verify system designs at early developmental stages.

238

239 **2. Numerical and experimental setup**

240 In this study, two types of combustion analysis were performed. First, a zero-dimensional chemical kinetic
241 analysis was performed using the Digital Analysis of Reaction Systems (DARS) [43]. DARS has been built
242 with the specific purpose of enabling detailed chemical kinetics analysis to engineering applications, with one

243 particular focus on internal combustion engines. It handles gas phase chemistry via a suite of reactor models
244 and reaction mechanisms. For this work we used a single-zone model for homogeneous-charge
245 compression-ignition (HCCI), rapid compression machine (RCM) model and free propagating flame model.
246 This analysis was performed to compare a new syngas chemical kinetics mechanism with existing mechanisms
247 and validated against the experiments performed with constant volume reactor, shock tube and RCM. Several
248 characteristics of syngas combustion were compared, such as, ignition delay, flame propagation, in-cylinder
249 pressure and temperature. For DARS HCCI analysis the intake-valve closure (IVC) time was 135 crank-angle
250 degrees (CA°) before top dead centre (BTDC), and the simulation was run for 265 CA° . The gas mixture
251 pressure and temperature at IVC were 225 kPa and 450 K, respectively. DARS RCM analysis was performed
252 at compression pressures (2-80bar) and temperatures (450-1000K). To calculate the laminar flame speed, free
253 propagating flame model was used at pressures (1-80bar) and temperatures (298-1000K).

254 Second, a multidimensional CFD analysis was performed using the Star-CD V4.2 code simulating the
255 combustion in a water-cooled four-stroke single-cylinder engine with two intake and two exhaust valves,
256 described in detail in [17]. In this engine, the autoignition of a small quantity of diesel pilot fuel, injected into
257 the combustion chamber before top dead centre (TDC), initiates the combustion. The burning diesel fuel then
258 ignites the gaseous fuel. A commercial solenoid-type injector that is typically used for diesel-only operations
259 was modified to ensure that only a small quantity of fuel was injected. The seven-hole nozzle of the
260 commercial injector was replaced by one with four holes, 0.1 mm in diameter. The diesel-fuel injection timing
261 and duration were controlled through signals transferred to the injector from the injector driver. A common-rail
262 injection system was employed to supply a constant injection pressure of 80 MPa to the injector. The quantity
263 of injected pilot diesel fuel was 1.2 mg/cycle. The simulations began from the intake valve closure at 135° CA
264 BTDC and were carried until 130° CA after top dead centre (ATDC). The simulation conditions with the
265 engine specifications and different types of primary gaseous fuel compositions used in this study are given in
266 Tables 1 and 2, respectively. This version of Star-CD incorporates the CHEMKIN code to formulate the

267 gas-phase chemistry with an advanced solver approach. The Star-CD code provides CHEMKIN with the
268 thermodynamic information for the computational cells, and the CHEMKIN code returns the new species
269 information after solving the chemistry. After solutions are obtained for all cells, the mass transfer, heat
270 transfer, and flow between cells are simulated by the corresponding sub-models. Then, the interactions
271 between the turbulent mixing and the chemical reactions are implemented. The CFD model was based on the
272 Reynolds-averaged governing equations; it was set to account for turbulence, the liquid fuel-injection spray,
273 and chemical mechanisms and was used the experimental conditions. The standard high-Reynolds number $k-\epsilon$
274 model was used for the turbulence modelling. A constant temperature of 450 K was used for the cylinder wall
275 and cylinder head, and 500 K was used for the piston surface. The pressure-implicit split-operator (PISO)
276 algorithm was used to simulate the transient flow of the engine. The injection process included the flow in the
277 nozzle hole and the atomisation process. The properties of atomisation and secondary break-up were calculated
278 by the Reitz–Diwakar model [44, 45]. To reduce the computation time, a 90° moving-sector mesh of 13,256
279 cells with cyclic boundaries was used to represent a bowl-in-piston configuration that was representative of the
280 experimental single-cylinder pilot-ignited dual-fuel engine [17]. A grid size between 0.5 and 2.0 mm and a
281 time step of 0.1° CA provided good numerical accuracies and computation stabilities. The sensitivity of the
282 grid was validated by comparing the motoring in-cylinder pressure histories from experiments.

283
284

285 **3. Development of the syngas kinetics mechanism**

286 Because the composition of syngas depends on the solid feedstock and its gasification process, it is very
287 challenging to develop a universal CFD-compatible syngas chemical kinetics mechanism that could cover the
288 broad range of engine combustion conditions. While developing syngas mechanism usually H_2/CO structure is
289 considered, however some syngas types derived from biomass and coke-oven solid feedstock may also include
290 CH_4 , as shown in this paper. Another complexity rises due to the effect of turbulence on combustion. Previous
291 studies showed that chemical kinetics mechanism with Chemkin models cannot accurately simulate engine

292 in-cylinder combustion and the effect of turbulence must be considered [41].

293 Therefore, for this research we have developed a CFD-compatible syngas chemical kinetics mechanism,
294 shown in Table 3, which can simulate dual-fuel engine combustion at various engine conditions, as shown in
295 Tables 1 and 2. The mechanism was compared with H₂/CO syngas mechanisms developed and validated
296 against experiments by other authors {Keromnes et.al. [35], Frassoldatti et al. [25] and GRI Mech 3.0 [32]}.
297 To consider CH₄ component in the syngas composition, the nine-step reduced mechanism for CH₄
298 autoignition by Li *et al.* [46] was used to add methane chemistry to H₂/CO reactions. To simulate the
299 pilot-injected diesel spray and ignition, the chemistry of C₇H₁₆ was included in the constructed mechanisms
300 as a single-step reaction, $C_7H_{16} + 11O_2 = 7CO_2 + 8H_2O$, based on an eddy breakup (EBU) mixing
301 representation by specifying the EBU reaction parameters [47]. Previous studies have shown that for
302 conventional diesel combustion, both diesel and C₇H₁₆ fuels show a similar ROHR [48]. This implies that
303 C₇H₁₆ is only used to initiate the pilot ignition of syngas. After the syngas is ignited, the combustion proceeds
304 without any C₇H₁₆ chemistry. The reason for this simplification is that the amount of injected diesel fuel was
305 1.2 mg/cycle, which provides only 2% of the total energy value in the cylinder, with negligible contribution to
306 the total ROHR. Previous results [17, 18] have shown that when micro-pilot injection is used, the ROHR
307 profiles do not include any changes due to the pilot diesel fuel combustion, which is opposite to what has
308 been found when the amount of pilot-injected fuel is high, as in [15]. Additionally, the experimental results
309 showed an undetectable level of soot formation during micro-pilot diesel fuel combustion.

310

311 *3.1 Sensitivity analysis*

312 A sensitivity analysis was performed for syngas Type 1 at temperature 1000K, equivalence ratio 0.63 and
313 pressure 10, 30 and 50 bar. In DARS, the sensitivity analysis is a representation of a simultaneous reaction
314 flow. Sensitivities are transported through the mechanism in the sense that a species is rated according to its
315 own importance and its involvement in producing or consuming important species [43]. The species

316 sensitivity, defined for each species, represents the sensitivity towards a chosen parameter A , and is the sum
 317 of the reaction sensitivities in which the species participate:

$$318 \quad S_{A,i}^S = \left| \sum_{k=1}^{N_r} \frac{\partial \psi_A}{\partial r_k} \cdot \frac{v'_{i,k}}{c_i} r_k \right| \quad (1)$$

319 Here $S_{A,i}^S$ contains the information on how sensitive an arbitrary parameter A in the vector of unknowns,
 320 $\partial \psi_A$, is to species i .

321 From sensitivity analysis the main hydrogen- and carbon-based reactions that play a key role were identified as
 322 shown in Figure 1. The importance of these reactions was also highlighted by other research groups [35, 42,
 323 49]. This analysis shows that $H_2O_2(+M)=OH+OH(+M)$, $H_2O_2+H=H_2+HO_2$ and $CO+H_2O=CO_2+H_2$ reactions
 324 contribute to the increasing reactivity of the mixture and $H_2+O=OH+H$, $O_2+CO=CO_2+O$ and
 325 $CH_4+OH=CH_3+H_2O$ reactions contribute to the decreasing reactivity. A brief description of importance of each
 326 of these reactions is given below.

327
 328 (R20) $H_2O_2(+M)=OH+OH(+M)$

329 The dissociation of H_2O_2 radicals is characterized by many researchers as the central kinetic feature in the
 330 operation of HCCI engines, or the key factor for the abnormal combustion phenomena, such as engine knock,
 331 in SI engines [49, 50]. This is because the decomposition of H_2O_2 via R20 gives access for secondary reactions
 332 and forms very reactive OH radicals [51]. Two different studies have been conducted to investigate the
 333 low-pressure limit and high-pressure limit rate constants. First Hong et al. [52], investigated R20 by using a
 334 laser absorption diagnostics for H_2O and OH [52, 53] at 1.8 atm pressure. Their results were in agreement with
 335 a previous study by Kappel et al. [51], although they have lower experimental uncertainty. They suggested a
 336 new lower-pressure limit rate constant for R20 and a high-pressure limit rate constant from a different study
 337 conducted by Sellevag [54]. The second study, conducted by Troe et al [55], suggests new pressure dependent
 338 rate constants by performing a theoretical study based on experimental data. Due to the lower level of
 339 experimental uncertainty Hong's set of rate constants has been adopted in this study for R20.

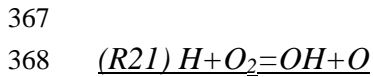
340 Other studies showed that at higher pressures, H_2O_2 concentration increases during $\text{H}_2\text{O}_2(+\text{M}) = \text{OH} +$
341 $\text{OH}(+\text{M})$ reaction [56]. This is because at higher pressures, the high concentration of the mixture, including
342 enhanced third-body efficiencies M, leads to a sufficient concentration of HO_2 , which is less reactive than
343 other free radicals, forming H_2O_2 . Before high temperatures are reached, the characteristic reaction time of
344 H_2/CO mixtures is long [34]. This reduction in reaction sensitivity causes the H_2O_2 concentration to increase. It
345 was also shown that as the equivalence ratio increases, the $\text{H}_2\text{O}_2/\text{OH}$ ratio gradually decreases and the higher
346 syngas initial H_2 concentration provides an enhanced chain-initiation process through $\text{H}_2 + \text{O}_2 \rightarrow \text{OH} + \text{OH}$ or
347 $\text{H}_2 + \text{O}_2 \rightarrow \text{H} + \text{HO}_2$ reactions, ensuring the occurrence of subsequent chain-branching reactions along with an
348 increase in the OH concentration.

349
350 (R24) $\text{H} + \text{O}_2(+\text{M}) \rightleftharpoons \text{HO}_2(+\text{M})$

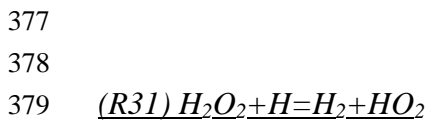
351
352 R24 has a key role in hydrogen combustion and is responsible for the reactivity at low temperatures [35].
353 Therefore, the temperature and pressure dependence of the chain propagation reaction R24 has been studied
354 extensively by many researchers [42]. Fernandes et al [57], proposed pressure and temperature dependent rate
355 constant for a temperature range between 300 -900 K and a pressure range between 1.5 to 900 bars. The
356 authors have tried to extend the temperature and pressure range by using the unimolecular rate theory.
357 However, at temperature ranges from 1000 to 1200 K, the mixture reactivity decreased significantly while the
358 ignition delay time increased. This is because of the low pressure limit rate constant which uses argon as a bath
359 gas. Bates et al. [58] studied the pressure and temperature dependence of R24 at temperature ranges from 1020
360 to 1260 K and pressure ranges from 10 to 50 bars by using argon. They proposed low pressure limit rate
361 constant that was in a good agreement with the experimental data.

362 Finally, during a new study by Keromnes et al. [35], a “hybrid” expression of rate constant was used by
363 combining the high pressure limit rate constants proposed by Fernandes [57] and the low pressure limit rate
364 constant proposed by Bates et al. [58]. The new hybrid rate constants showed a good agreement with the

365 experimental data at all the temperature and pressure ranges. Therefore, in our mechanism we adopted the new
366 rate constants proposed by Keromnes et al. [35].



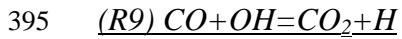
369 R21 is one of the most important reactions in the syngas chemical reaction mechanism. It is a leading reaction
370 which is responsible for the control of the fuels oxidation at temperatures higher than 1000 K [35]. Because of
371 its sensitivity, the rate constants used in different mechanisms vary. For example, the rate constant proposed by
372 Piraglia et al. [59] were adopted by Muller et al. [60] and Oconnair et al. [61], in order to reproduce more
373 accurate explosion limit at temperatures between 680-900 K. Other authors such as Keromnes et al. [35] used a
374 rate constant proposed by Hong et al. [62], which has 10% uncertainty at temperature ranges from 1100 to
375 3370 K. During this study the rate constant from Fernandes Gallisteo et al. [63] was adopted to show a good
376 agreement with the experimental results.



380 This reaction is very important under low temperatures and high pressure conditions. The consumption of one
381 HO_2 radical leads to the production of one H_2O_2 molecule. The decomposition of H_2O_2 will, in turn, lead to the
382 formation of two high reactive OH radicals [35]. Therefore it can be said that R31 is responsible for the
383 increase of the reactivity. Due to its high sensitivity this reaction has been studied in detail by many authors in
384 order to find the best rate constants [42]. The rate constants recommended by Tsang et al. [64] is by a factor of
385 3 higher than the rate constants recommended by Baulch et al. [65]. Different rate constants result in different
386 ignition delay times, as shown by Keromnes et al. [35]. For example at 50 bar and 1000K the ignition delay
387 times obtained by Baulch et al. [65] were by a factor of 3 different than the ignition delay times obtained by
388 Tsang et al. [64]. During a study by Ellingson et al. [66] the rate constants are calculated by using the canonical
389 variational transition state theory. The calculated ignition delay times from Ellingson approach were in a good
390 agreement with Mittal et al. calculations [67]. The rate constant recommended by Konnov [42] was adopted

391 with exponential factor $A = 7.7E12$, which lies within the stated level of uncertainty, in order to get the best
392 agreement of our mechanism with the experimental data and with the ignition delay times from other already
393 proposed mechanisms.

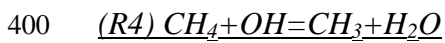
394



396 According to Li et al. [40], the laminar flame speed and the mixture reactivity are sensitive to R9 [68].

397 Therefore, in order to obtain the best agreement with the experimental data and the laminar flame speed
398 measurements the reaction constants proposed by Frassoldati et al. [25] were used in this study.

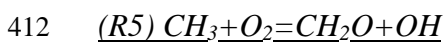
399



401 This reaction is responsible for the consumption of CH_4 and the formation of CH_3 radicals. Different rate
402 constants have been proposed in the literature and used in different chemical reaction mechanisms by different
403 researchers. The rate constant used for GRI Mech 3.0 [32] was based on the Cohen's Transition State Theory
404 and validated against experimental data [69]. Baulch et al. [70] also proposed a new rate constant based on the
405 study of Madronich and Felder [71] with an extended temperature range from 250 to 2500 K. Srinivasan et al.
406 [72] on the other hand proposed a new non-Arrhenius expression for a temperature range between 195-2025 K.
407 Li and Williams [73] used a rate constant for R4 which shows a good level of accuracy and it was in a good
408 agreement with the measured and calculated data. In our study we used the rate constant from Li and Williams
409 [73] which gave a good match with our experimental results.

410

411



413 One of the most important reactions for the accurate prediction of methane ignition delay time is R5 [74]. The
414 importance of that reaction forced researchers to investigate in detail the temperature and pressure dependence
415 of R5 and propose different rate constants. For example, the rate constant used in San Diego mechanism [75] is
416 higher by a factor of forty-two from the rate constant used in GRI Mech 3.0 [32]. The rate constant proposed
417 by Srinivasan et al. [76], is one order of magnitude lower than the rate constant suggested by Herbon et al. [77].

418 In our mechanism we used the rate constants proposed by Frassoldati et al. [25].

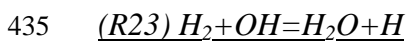
419



421 The consumption and the production of hydrogen radicals play a key role on the ignition delay times and the
422 laminar flame speed and in general are very important for the in-cylinder combustion. Therefore, reactions
423 which are responsible for the production of H radicals have been investigated in deep by different researchers
424 in order to find the most accurate rate constant during low and high temperature and pressure conditions.
425 R22 is responsible for the production of H and OH radicals. The production of OH radicals leads to the
426 initiation of reaction R23 which will be discussed in the next paragraph. According to a review by Baulch et al.
427 [78], the most accurate rate constant for R22 was proposed by Sutherland et al. [79]. The expression from
428 Sutherland is compared with the measurements from Natarajan and Roth [80] at temperature range from 1713
429 to 3532 K, with Davidson and Handson [81] validated at ranges from 2120-2750 K and finally tested by Javoy
430 et al. [82] at temperatures 2690-3360 K. For all of the temperature ranges the expression proposed by
431 Sutherland showed a very good agreement with the measurements. During this study we used the rate constant
432 which were proposed by Sutherland [79].

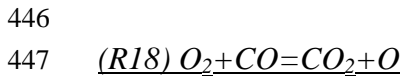
433

434

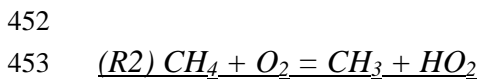


436 The production of OH radicals from R22, triggers R23. The reaction between H_2 and OH radicals leads to the
437 conversion of OH to H atoms. Laminar flame speed and ignition delay times are also very sensitive to this
438 reaction [83]. Many researchers investigated the rate constants and proposed a value to accurately predict the
439 sensitivity of this reaction to the temperature changes. For temperature ranges between 300 and 2500 K,
440 Baulch et al. [78] proposed a new rate constant which was used also by Konnov [84, 85]. However, a second
441 research by Baulch et al. [65] based on the work of Michael et al. [86] and Oldenberg et al. [87], showed that
442 R23 is very sensitive to the temperature changes. At 300 K the uncertainty factor of R23 was 1.2 increasing to
443 2 at temperature 2500 K [65]. Therefore, a new rate constant has been proposed by Baulch et al. [65] in order

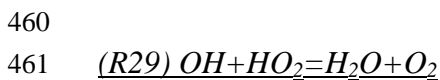
444 to satisfy the uncertainty of R23 at different temperatures. In this study we used the rate constant proposed by
445 Sutherland et al. [79].



448 According to a research by Saxena et al. [20], although reaction 18 does not affect the laminar burning
449 velocities, it is very important for the ignition initiation and the ignition delay times especially at lower
450 hydrogen content. This reaction is therefore an essential reaction and is added to the mechanisms by using the
451 rate constant from Frassoldati et al [25].



454 The preignition chemistry of methane is initiated primarily by this reaction. At high pressures or in the initial
455 stages of hydrocarbon oxidation, high concentrations of HO_2 can initiate reaction $CO + HO_2 = CO_2 + OH$ [88].
456 Thus, CO oxidation at high pressures can be modelled by adding reaction $CO + HO_2 = CO_2 + OH$ to the syngas
457 kinetics mechanism, as shown by Kim *at al.* [89]. This reaction is the most sensitive of the CO subsystems
458 under the conditions investigated. The rate constant used for this reaction was updated taking the rate constant
459 from Li and Williams [46] that was originally proposed by Lindstedt and Skevis [90].



462 A recent study by Keromnes et al. [35] showed that R29 is very sensitive to the fuel-lean flames. Many
463 theoretical and experimental studies have been conducted in order to analyse the dependency of the reaction
464 rate constants on the temperature [66, 91-92]. However, at temperatures around 1250 K, unusual temperature
465 dependence is observed which leads to a non-Arrhenius behaviour and creates a deep minimum for the
466 calculated rate constant [35]. This makes the reproduction of the temperature dependence very difficult and
467 creates high level of uncertainties [42]. Recent investigations by Hong et al. [93] and Burke et al. [92], showed
468 that R29 has a weak temperature dependence but they also concluded that future work is required to ensure the
469 accuracy of the rate constants at temperatures between 900-1200 K. In this study we used rate constants
470 defined by Keromnes et al. [35].

471

472 *3.2 Ignition delay*

473

474 Ignition delay time simulations were performed using RCM model in DARS. Ignition delay time obtained
475 using the new mechanism was compared with that obtained by Keromnes et al. [35], Frassoldati et al. [25] and
476 GRI Mech 3.0 [32] for four types of syngas compositions at $T=800-1053\text{K}$, $P=225\text{kPa}$ and $\phi=0.63$. Figure 2
477 shows that the ignition delay time for the new mechanism matches very well with those obtained using
478 different tested mechanisms in the broad range of temperatures for all syngas types investigated in this paper.
479 Figures 3 and 4 show the ignition delay times for new mechanism at high pressures. Analysis was performed
480 for syngas type 1 at temperature range $800-1053\text{K}$ and $\phi=0.63$, and syngas type 2 at temperature range
481 $800-1053\text{K}$ and $\phi=0.83$. The results obtained by using new mechanism were in a good agreement with the
482 ignition delay times obtained by using Frassoldati et al. [25] and Keromnes et al. [35] mechanisms and in
483 exceptionally good agreement with ignition delay times obtained by using GRI Mech 3.0 [32] mechanism.

484 We also compared the ignition delay times using syngas mixture compositions defined in Table 4 from the
485 University of Connecticut. The study has been performed under stoichiometric conditions with 50%, 25% and
486 10% H_2 in the H_2/CO fuel mixtures at the end-of-compression temperature range of $914-1068\text{K}$ using the new
487 mechanism and mechanism reported by Keromnes et al. [35]. Results on Figure 5 show the inhibiting effect of
488 carbon monoxide on the syngas ignition delay times, which increase with increasing amounts of CO in the
489 syngas mixture. The new mechanism captures this inhibiting effect accurately and its predictions are in a very
490 good agreement.

491

492

493 *3.3 Flame speed*

494

495 The flame speed analysis was performed to compare the laminar flame speed obtained using the new
496 mechanism with that of Keromnes et al. [35], Frassoldati et al. [25] and GRI Mech 3.0 [32]. Figure 6 shows
497 that for syngas types 1-4 over a range of equivalence ratios, the new mechanism showed the identical trend in

498 laminar flame speed as the one obtained using above mentioned mechanisms. For syngas type 4, GRI Mech
499 3.0 mechanism slightly over predicted the laminar flame speed. This is due to the high H₂ concentration in the
500 type 4 syngas. GRI Mech 3.0 was developed to simulate mainly natural gas combustion and was not designed
501 to predict the oxidation of fuel with high H₂ content. Figure also shows that laminar flame speed for syngas
502 type 2 is slightly higher due to higher H₂ concentration compared to syngas types 1 and 3.

503 Using new mechanism we evaluated laminar flame speed for H₂/CO/CO₂ mixtures and compared the
504 results with experimental data by Hu et al. [94] and predictions from the different kinetics models [25, 32, 35]
505 over a range of equivalence ratios, $\phi=0.4-1.0$. Figure 7 shows the flame speed calculated using the chemical
506 kinetics mechanisms for H₂/CO/CO₂ – 35:35:30 mixture at different pressures and temperatures. The new
507 mechanism performed remarkably well at predicting the laminar flame speed across all the equivalence ratios
508 investigated by Hu et al. [94].

509 In this study, we also considered the laminar flame speed of H₂/CH₄ at a range of CH₄ ratios and
510 equivalence ratios to evaluate the new mechanism. Figure 8 shows the laminar flame speed for various H₂:CH₄
511 ratios at T=298K and P=1atm and equivalence ratio ranging from 0.4 to 1.2. For H₂/CH₄ mixtures the laminar
512 flame speed results obtained with the new mechanism exhibit the best agreement with the laminar speed data
513 obtained using Keromnes et al. [35] and GRI Mech 3.0 [32] mechanisms.

514 Laminar flame speed was also evaluated at high pressures. Figure 9 shows that at P=20 bar the laminar
515 speed data obtained using the new mechanism matches well with those obtained using GRI Mech 3.0
516 mechanism, showing slight deviation from the laminar flame speed obtained using Keromnes et al. [35] and
517 Frassoldati et al. [25] mechanisms. However, this difference gradually disappears at lower equivalence ratio
518 levels, those usually used in dual-fuel engine combustion. At high pressure of 80 bar the laminar flame speed
519 data matches well for all tested mechanisms and equivalence ratios.

520
521 **4. Results and Discussion**
522

523 *4.1 Mechanism validation for CFD combustion analysis*

524 To validate the mechanism for the engine in-cylinder-like conditions in a dual-fuel engine, an analysis was
525 performed by applying a pilot injection using the coupled CFD and syngas chemical kinetics mechanism.
526 Figure 10 compares the in-cylinder pressure obtained by a new mechanism using CFD code with that of
527 Slavinskaya et al. [27], Keromnes et al. [35], Frassoldatti et al. [25], GRI Mech 3.0 [32] and engine experiment.
528 Figure 10 shows that new mechanism accurately simulates the engine in-cylinder combustion for syngas with
529 different compositions where other syngas mechanisms show very large deviation from experiments. A similar
530 trend was observed for a range of different equivalence ratios and injection timings.

531

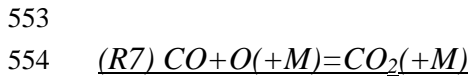
532 *4.2 Chemical kinetics mechanism for syngas with high H2 content*

533 The developed mechanism showed good match between simulation results and experimental data for
534 syngas Types 1-3 (biomass solid feedstock) at various equivalence ratios and injection timings. However, with
535 this mechanism the combustion rate was much higher for syngas Type 4 (coke-oven solid feedstock). The
536 higher combustion rate was due to the effect of higher H₂, higher CH₄ and lower CO gas concentrations.

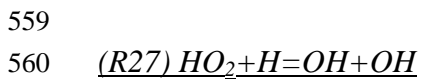
537 The rate constants for reaction $\text{H}_2\text{O}_2 + \text{H} = \text{H}_2 + \text{HO}_2$ were replaced by constants from different mechanisms
538 as it was expected that with higher H₂ concentration the in-cylinder combustion rate would be affected by this
539 reaction. This reaction is very important under low temperature and high pressure conditions. The consumption
540 of one HO₂ radical leads to the production of one H₂O₂ molecule. The decomposition of H₂O₂ will, in turn,
541 lead to the formation of two high reactive OH radicals via $\text{H}_2\text{O}_2 (+\text{M}) = \text{OH} + \text{OH} (+\text{M})$ [35]. Due to its high
542 sensitivity H₂O₂+H=H₂+HO₂ reaction has been studied in detail by many authors in order to find the
543 best-matching rate constants [42]. In fact, we can find a great variety in rate constant values used for different
544 syngas chemical kinetic mechanisms. Konnov [42] proposed a new rate constant for reaction
545 $\text{H}_2\text{O}_2 + \text{H} = \text{H}_2 + \text{HO}_2$ which is based on a new research by Baulch et al. [65]. Konnov [42] reevaluated
546 $\text{H}_2\text{O}_2 + \text{H} = \text{H}_2 + \text{HO}_2$ rate constants and increased the uncertainty factor to 3.

547 We performed the reaction sensitivity study using the modified mechanism for syngas with a higher H₂

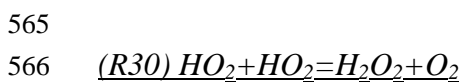
548 content. It shows the high sensitivity of $H_2O_2(+M)=OH+OH(+M)$, $H_2O_2+H=H_2+HO_2$, and
549 $HO_2+HO_2=H_2O_2+O_2$ reactions and low sensitivity of $HO_2+H=OH+OH$ reaction. It should be noticed that
550 reactions R7, R27 and R30 were not shown as sensitive in Figure 1 when the original mechanism was applied
551 to syngas type 1 (H_2 -13.7%), and showed strong sensitivity in Figure 11 when modified mechanism was
552 applied to syngas type 4 (H_2 -56.8%). Brief description of these three reactions is given below:



555 R7 is responsible for the conversions of CO to CO_2 and is very sensitive at high pressures and high
556 temperatures. In order to estimate accurately the dependence of R7 on the temperature and pressure, low
557 pressure limit rate constants must be used [95]. For this research we used the high and low pressure limit rate
558 constants which were proposed by Frassoldati et al. [25] and validated against experimental data.



561 According to O'Conaire et al. [96], changing the rate constant of R27 has an adverse effect on the results of the
562 flow reactor simulations. They suggested a rate constant for R27 which is within the limits of the experimental
563 data obtained from the NIST database [97], and has lower uncertainty factor. In this paper the rate constants
564 proposed by O'Conaire [96] were adopted because they are within the limits of the experimental data.



567 This reaction is very sensitive during low temperature and high pressure conditions [98]. Both reactions, R30
568 with R31, contribute to the formation of H_2O_2 which in turn decomposes into two highly reactive OH radicals
569 through reaction R20. However, it can be said that R30 and R31 are competitors; in which R30 increases the
570 reactivity as it produces two HO_2 radicals while R31 inhibits the reactivity as it produces only one HO_2 radical.
571 The set of rate constants used by Keromnes et al. [35] was chosen for this study.

572 Comparison of two sensitivity analysis for Type 1 shown in Figure 1 and Type 4 shown in Figure 11
573 suggests that for Type 1, with lower H_2 content, more carbon-based reactions play important role in chemical
574 kinetics, whereas, for Type 4 with higher H_2 content the number of hydrogen-based sensitive reactions

575 prevailed. Figures 12 and 13 show the flow of species of carbon and hydrogen in syngas Type 1 and Type 4. It
576 is seen that for carbon atoms of both syngas types, the major paths represent the high-temperature hydrocarbon
577 oxidation of CH_4 through CH_3 and further oxidation of CH_3 to CH_2O .

578 Fluxes for H below 1% of maximum flow have been filtered. The flow analysis for hydrogen species at
579 lower H_2 content of syngas (Type 1, Type 2 and Type 3) showed the identical flow pattern at pressures 10, 30
580 and 50 bar as shown in Figure 13. However, when hydrogen concentration in the syngas increases more than
581 50 % (Type 4) flow from H_2O_2 to OH and back increases as the pressure increases. It was observed that at high
582 pressures the effect of H atom becomes noticeable to contribute to HO_2 formation.

583 Ignition delay time and laminar flame speed obtained using modified mechanism were compared with
584 those obtained using Keromnes et al. [35], Frassoldati et al. [25] and GRI Mech 3.0 [32] and the new
585 mechanism. Figure 14 shows that modified mechanism that is tend to simulate syngas with high H_2
586 concentration accurately predicted ignition delay and laminar flame speed. To estimate the effect of different
587 rate constants on the in-cylinder heat production and pressure rise, the mechanism was tested by running 3D
588 CFD analysis with reaction rate constants proposed by different authors. Figure 15 shows in-cylinder pressure
589 CFD results for syngas composition of Type 4. $\text{H}_2\text{O}_2+\text{H}=\text{H}_2+\text{HO}_2$ reaction constants proposed by Hong et al.
590 [49] and adjusted power factor $n = 0.0$ showed the closest match with experimental data.

591

592 *4.3 In-cylinder 3D combustion analysis*

593 To validate the new mechanism shown in Table 3 for the in-cylinder-like conditions in a dual-fuel engine,
594 an analysis was performed by applying a micro-pilot injection using the coupled CFD and developed syngas
595 chemical kinetics mechanism. The pressure and ROHR plots shown in Figure 16 show a good match between
596 the simulation results and experimental data for different types of syngas at various equivalence ratios and
597 injection timings. Conditions A-B, C-D and E-F were simulated using the new chemical kinetics mechanism,
598 and conditions G-H were simulated using the modified mechanism with constants for reaction R31 adopted

599 from Hong et al. [49] with adjusted power factor $n = 0.0$. Figure 17 shows the crank angle resolved in-cylinder
600 spray and temperature distribution for syngas type 1 and type 4. The images show micro-pilot injected
601 n-heptane spray development with further ignition and combustion of syngas. The maximum in-cylinder
602 spatial temperature reached about 2200K and it is seen that the flame front propagates towards the cylinder
603 wall gradually consuming the unburned in-cylinder mixture and the fuel is fully burned. The files with
604 animation of the full combustion process for these two conditions are attached to this manuscript as
605 supplementary material.

606

607 **5. Conclusion**

608 This study presents a new CFD-compatible syngas chemical kinetics mechanism based on the flow and
609 reaction sensitivity analysis and CFD simulations. The developed syngas mechanism was validated in a
610 supercharged dual-fuel engine with various syngas initial compositions under lean conditions concurrently by
611 using a chemical kinetics code and a multidimensional CFD code. The results were compared with
612 experimental data of combustion and syngas chemical kinetics mechanisms developed by other researchers.
613 Ignition delay time and laminar flame speed results predicted by using the new mechanism are in a very good
614 agreement with those obtained by using other validated syngas mechanisms. Sensitivity analysis showed that
615 the reactivity of syngas mixtures was found to be governed by hydrogen and CO chemistry for H_2
616 concentrations lower than 50% and mostly by hydrogen chemistry for H_2 concentrations higher than 50%. In
617 the mechanism validation, particular emphasis is placed on predicting the combustion under high pressure
618 conditions. For high H_2 concentration in syngas under high pressure, the reactions $HO_2+HO_2=H_2O_2+O_2$ and
619 $H_2O_2+H=H_2+HO_2$ were found to play important role affecting the in-cylinder combustion rate and heat
620 production. The rate constants for $H_2O_2+H=H_2+HO_2$ reaction showed strong sensitivity to high-pressure
621 ignition times and has considerable uncertainty. To accurately simulate syngas derived from coke-oven
622 feedstock with high H_2 concentration some modifications to a new mechanism were introduced. In particular,

623 constants for reaction R31 were adopted from Hong et al. [49] with adjusted power factor $n = 0.0$. and
624 reactions $\text{HO}_2 + \text{OH} = \text{H}_2\text{O} + \text{O}_2$ and $\text{O} + \text{H}_2\text{O} = \text{OH} + \text{OH}$ were excluded from the mechanism. These reactions did
625 not appear in the list of the most sensitive reactions. In fact, they are not contributing to the further chain
626 branching and chain propagation where H radical presence is required.

627 Developed mechanism was used in CFD analysis to predict in-cylinder combustion of syngas and results
628 were compared with experimental data. The new mechanism predicted the in-cylinder combustion
629 performance well for both biomass and coke-oven syngas in a micro-pilot ignited supercharged dual-fuel
630 engine, including the cylinder pressure history and heat-release rate data with respect to syngas composition,
631 equivalence ratio, and injection timing.

632

633 **Acknowledgements**

634 The authors are grateful to the Faculty of Engineering and Environment of Northumbria University for
635 providing funding for this work through RDF studentship.

636

637

638 The English in this document has been checked by at least two professional editors, both native speakers of
639 English.

640

641

642 **References**

643 [1] Sridar G, Paul PJ, Mukunda HS. Biomass derived producer gas as a reciprocating engine fuel-an
644 experimental analysis. *Biomass and Bioenergy* 2001;21:61-72.

645 [2] Shilling NZ, Lee DT. IGCC-Clean power generation alternative for solid fuels: GE Power Systems.
646 *PowerGenAsia* 2003.

647 [3] Shudo T, takahashi T, Influence of reformed gas composition on HCCI combustion engine system fueled
648 with DME and H_2 -CO-CO₂ which are onboard-reformed from methanol utilizing engine exhaust heat.
649 *Trans.JSME B* 2004;70:2663.

650 [4] Shudo T. An HCCI combustion engine system using on-board reformed gases of methanol with waste heat
651 recovery: Ignition control by hydrogen. *Int J Veh Design* 2006;41:206.

652 [5] Li H, Karim GA. Exhaust emissions from an SI engine operating on gaseous fuel mixtures containing
653 hydrogen. *Inj J Hydrogen Energy* 2005;30:1491.

654 [6] Karim G.A. Combustion in gas fueled compression: Ignition engines of the dual fuel type. *J. Eng. Gas Turb.*

- 655 Power 2003;125:827-836.
- 656 [7] Liu Z, Karim GA. Simulation of combustion process in gas-fuelled diesel engine. Proc Inst Mech Eng
657 A:11.
- 658 [8] Poonia MP, Ramesh A, Gaur RR. Effect of intake air temperature and pilot fuel quantity on the combustion
659 characteristics of a LPG-diesel dual-fuel engine. SAE Paper, 982455.
- 660 [9] Karim GA, Moore NPW. The production of hydrogen by the partial oxidation of methane in a dual-fuel
661 engine. SAE Paper, 901501.
- 662 [10] Karim GA, Wierzbka I. Safety measures associated with the operation of engines on various alternative
663 fuels. Reliability Eng Syst Safety 1992;37:93.
- 664 [11] McMillian MH, Lawson SA. Experimental and modeling study of hydrogen/syngas production and
665 particulate emissions from a natural gas-fuelled partial oxidation engine. Int J Hydrogen Energy 2006;31:847.
- 666 [12] Christodoulou F, Megaritis A. The effect of reformer gas mixture on the performance and emissions of an
667 HSDI diesel engine. Int J Hydrogen Energy 2014;39:9798.
- 668 [13] Bilcan A. Contribution to the study of the thermodynamic cycle of dual-fuel. PhD Thesis 2003, Nantes
669 University, France.
- 670 [14] Baratieri M, Baggio P, Bosio P, Grigiante M, Longo GA. The use of biomass syngas in IC engines and
671 CCGT plants: A comprehensive analysis. Applied Therm Engineering 2009;29:3309-3318.
- 672 [15] Boehman AL, Le Corre O. Combustion of syngas in internal combustion engines. Combust Sci Tech
673 2008;180:1193-1206.
- 674 [16] Tomita E, Fukatani N, Kawahara N, Maruyama K, Komoda T. Combustion characteristics and
675 performance of supercharged pyrolysis gas engine with micro-pilot ignition. CIMAC congress 2007. Paper No.
676 178.
- 677 [17] Roy MM, Tomita E, Kawahara N, Harada Y, Sakane A. Performance and emission comparison of a
678 supercharged dual-fuel engine fueled by producer gases with varying hydrogen content. Int J Hydrogen Energy
679 2009;34:7811-22.
- 680 [18] Roy MM, Tomita E, Kawahara N, Harada Y, Sakane A. Performance and emissions of a supercharged
681 dual-fuel engine fueled by hydrogen-rich coke oven gas. Int J Hydrogen Energy 2009;34:9628-38.
- 682 [19] Yetter RA, Dryer FL, Rabitz H. A comprehensive reaction mechanism for carbon
683 monoxide/hydrogen/oxygen kinetics. Combust Sci Tech 1991;79:97.
- 684 [20] Saxena P, Williams FA. Testing a small detailed chemical-kinetic mechanism for the combustion of
685 hydrogen and carbon monoxide. Combust Flame 2006;145:316-323.
- 686 [21] Dowdy DR, Smith DB, Taylor SC, Williams A. The use of expanding spherical flames to determine
687 burning velocities and stretch effects in hydrogen-air mixtures. Proc Combust Inst 1990; 23:325.
- 688 [22] Egolfopoulos FN, Law CK. An experimental and computational study of the burning rates of ultra-lean to
689 moderately rich H₂/O₂/N₂ laminar flames with pressure variations. Proc Combust Inst 1990;23:333.
- 690 [23] Tse SD, Zhu DL, Law CK. Morphology and burning rates of expanding spherical flames in H₂/O₂/inert
691 mixtures up to 60 atmospheres. Proc Combust Inst 2000;28:1793.
- 692 [24] Kwon OC, Faeth GM. Flame/stretch interactions of premixed hydrogen-fueled flames: measurements and

693 predictions. *Combust Flame* 2001;124:590.

694 [25] Frassoldati A, Faravelli T, Ranzi E. The ignition, combustion and flame structure of carbon
695 monoxide/hydrogen mixtures. Note 1: Detailed kinetic modeling of syngas combustion also in presence of
696 nitrogen compounds. *Int J Hydrogen Energy* 2007;32:3471-3485.

697 [26] Cuoci A, Frassoldati A, Buzzi Ferraris G, Faravelli T, Ranzi E. The ignition, combustion and flame
698 structure of carbon monoxide/hydrogen mixtures. Note 2: Fluid dynamics and kinetic aspects of syngas
699 combustion. *Int J Hydrogen Energy* 2007;32:3486-3500.

700 [27] Slavinskaya N, Braun-Unkhoff M, Frank P. Reduced reaction mechanisms for methane and syngas
701 combustion in gas turbines. *J Engr Gas Turb Power* 2008;130:(021504)1-6.

702 [28] Starik AM, Titova NS, Sharipov AS, Kozlov VE. Syngas oxidation mechanism. *Combust Expl Shock*
703 *Waves* 2010;46:491-506.

704 [29] Sun H, Yang SI, Jomaas G, Law CK. High-pressure laminar flame speeds and kinetic modeling of carbon
705 monoxide/hydrogen combustion. *Proc Combust Inst* 2007;31:439-446.

706 [30] Sivaramakrishnan R, Comandini A, Tranter RS, Brezinsky K, Davis SG, Wang H. Combustion of CO/H₂
707 mixtures at elevated pressures. *Proc Combust Inst* 2007;31:429-437.

708 [31] Cavaliere DE, De Ioannon M, Sabia P, Allegorico M, Marchione T, Sirignano M, D'Anna A. A
709 comprehensive kinetic modeling of ignition of syngas/air mixtures at low temperatures and high pressures.
710 *Combustion Colloquia 2009, 32nd Meeting on Combustion of the Italian Section of the Combustion Institute,*
711 *April 26-28, Napoli, University Federico II, 26-28 of April, 2009.*

712 [32] Smith GP, Golden DM, Frenklach M, Moriarty NW, Eiteneer B, Goldenberg M, Bowman CT, Hanson RK,
713 Song S, Gardiner WC, Jr., Lissianski VV, and Qin Z GRI-Mech home page
714 http://www.me.berkeley.edu/gri_mech/

715 [33] Mittal G, Sung CJ, Fairweather M, Tomlin AS, Griffiths JF, Hughes KJ. Significance of the HO₂+CO
716 reaction during the combustion of CO+H₂ mixtures at high pressures. *Proc Combust Inst* 2007;31:419-427.

717 [34] Chaos M, Fryer FL. Syngas combustion kinetics and applications. *Combust Sci Tech*
718 2008;180:1053-1096.

719 [35] Kéromnès A, Metcalfe WK, Heufer KA, Donohoe N, Das AK, Sung CJ, Herzler J, Naumann C, Griebel P,
720 Mathieu O, Krejci M, Petersen EL, Pitz WJ, Curran HJ. An experimental and detailed chemical kinetics
721 modeling study of hydrogen and syngas mixture oxidation at elevated pressures. *Combust Flame*
722 2013;160:995-1011.

723 [36] Lee HC, Mohamad AA, Jiang LY. Comprehensive comparison of chemical kinetics mechanisms for
724 syngas/biogas mixtures. *Energy Fuels* 2015;29:6126-6145.

725 [37] Metcalfe WK, Burke SM, Ahmed SS, Curran HJ. A Hierarchical and Comparative Kinetic Modeling
726 Study of C₁ – C₂ Hydrocarbon and Oxygenated Fuels. *Int J Chem Kinet* 2013;45:638-675.

727 [38] Olm C, Zsely IG, varga T, Curran HJ, Turanyi. Comparison of the performance of several recent syngas
728 combustion mechanisms. *Combust Flame* 2015;162:1793-1812.

729 [39] Healy D, Kalitan DM, Aul CJ, Petersen EL, Bourque G, Curran HJ. Oxidation of C₁-C₅ Alkane
730 Quinternary Natural Gas Mixtures at High Pressures. *Energy Fuels* 2010;24:1521-1528.

731 [40] Li J, Zhao Z, Kazakov A, Chaos M, Dryer FL, Scire JJJ. A comprehensive kinetic mechanism for CO,

732 CH₂O, and CH₃OH combustion. *Int J Chem Kinet* 2007;39:109-136.

733 [41] Kong SC, Reitz RD. Use of detailed chemical kinetics to study HCCI engine combustion with
734 consideration of turbulent mixing effects. *J Eng Gas Turb Power* 2002;124:702-707.

735 [42] Konnov A. Remaining uncertainties in the kinetic mechanism of hydrogen combustion. *Combust Flame*
736 2008;152:507-528.

737 [43] 2015 CD-Adapco Inc., DARS Basic 2.10.

738 [44] Reitz RD, Diwakar R. Effect of drop breakup on fuel sprays. SAE paper, 860469.

739 [45] Reitz RD, Diwakar R. Structure of high-pressure fuel spray. SAE paper, 870598.

740 [46] Li SC, Williams FA. A reduced reaction mechanism for predicting knock in dual-fuel engines. SAE Paper
741 2000-01-0957.

742 [47] 2015 CD-Adapco Inc. Methodology, Star-CD V4.2

743 [48] Donkerbroek AJ, van Vliet AP, Somers LMT, Frijters PJM, Klein-Douwel RJH, Dam NJ, Meerts WL, ter
744 Meulen JJ. Time- and space-resolved quantitative LIF measurements of formaldehyde in a heavy-duty diesel
745 engine. *Combust Flame* 2010;157:155-166.

746 [49] Hong Z, Davidson DF, Hanson RK. An improved H₂/O₂ mechanism based on recent shock tube/laser
747 absorption measurements. *Combust Flame* 2011;158:633-644.

748 [50] Westbrook CK. Chemical kinetics of hydrocarbon ignition in practical combustion systems. *Proc.*
749 *Combust. Inst* 2000;28:1563-1577.

750 [51] Kappel C, Luther K, Troe J. Shock wave study of the unimolecular dissociation of H₂O₂ in its falloff
751 range and of its secondary reactions. *Phys Chem Chem Phys* 2002;4:4392-4398.

752 [52] Hong Z, Farooq A, Barbour EA, Davidson DF, Hanson RK. Hydrogen peroxide decomposition rate: A
753 shock tube study using tunable laser absorption of H₂O near 2.5 μm. *J Phys Chem* 2009;113:12919-12925.

754 [53] Hong Z, Cook RD, Davidson DF, Hanson RK. A shock tube study of OH + H₂O₂ → H₂O + HO₂ and
755 H₂O₂ + M → 2OH + M using laser absorption of H₂O and OH. *J Phys Chem* 2010;114:5718-5727.

756

757 [54] Sellevag SR, Georgievskii Y, Miller JA. Kinetics of the gas phase recombination reaction of hydroxyl
758 radicals to form hydrogen peroxide. *J Phys Chem* 2009;113:4457-4467.

759

760 [55] Troe J. The thermal dissociation/recombination reaction of hydrogen peroxide H₂O₂(+M) ↔ 2OH(+M)
761 III. Analysis and representation of the temperature and pressure dependence over wide ranges. *Combust. Flame*
762 2011;158:594-601.

763

764 [56] Azimov U, Okuno M, Tsuboi K, Kawahara N, Tomita E. Multidimensional CFD simulation of syngas
765 combustion in a micro-pilot-ignited dual-fuel engine using a constructed chemical kinetics mechanism. *Int J*
766 *Hydrogen Energy* 2011;36:13793-13807.

767

768 [57] Fernandes RX, Luther K, Troe J, Ushakov VG. Experimental and modelling study of the recombination
769 reaction H + O₂(+M) → HO₂(+M) between 300 and 900 K, 1.5 and 950 bar, and in the bath gases M = He, Ar,
770 and N₂. *Phys Chem Chem Phys* 2008;10:4313-4321.

771

- 772 [58] Bates RW, Golden DM, Hanson RK, Bowman CT. Experimental study and modeling of the reaction $H +$
773 $O_2 + M \rightarrow HO_2 + M$ ($M = Ar, N_2, H_2O$) at elevated pressures and temperatures between 1050 and 1250 K.
774 *Phys Chem Chem Phys* 2001;3:2337–2342.
775
- 776 [59] Pirraglia AN, Michael JV, Sutherland JW, Klemm RB. A flash photolysis-shock tube kinetic study of the
777 H-atom reaction with O_2 : $H + O_2 \rightarrow OH + O$ ($962 \leq T \leq 1705$ K) and $H + O_2 + Ar \rightarrow HO_2 + Ar$ ($746 < T <$
778 987 K). *J Phys Chem* 1989;93:282–291.
779
- 780 [60] Mueller MA, Kim TJ, Yetter RA, Dryer FL. Flow reactor studies and kinetic modeling of the
781 H_2/O_2 reaction. *Int J Chem Kinet* 1999;31:113–125.
782
- 783 [61] O’Conaire M, Curran HJ, Simmie JM, Pitz WJ, Westbrook CK. A comprehensive modeling study of
784 hydrogen oxidation. *Int J Chem Kinet* 2004;36:603–622.
785
- 786 [62] Hong Z, Davidson DF, Barbour EA, Hanson RK. A new shock tube study of the $H + O_2 \rightarrow OH + O$
787 reaction rate using tunable diode laser absorption of H_2O near $2.5 \mu m$. *Proc. Combust Inst* 2011;33:309–316.
788
- 789 [63] Fernandez-Galisteo D, del Alamo G, Sanchez AL, Linan A. Zeldovich analysis of hydrogen-air premixed
790 flames. In: *Proceedings of the European Combustion Meeting 2007*.
791
- 792 [64] Tsang W, Hampson RF. Chemical kinetic database for combustion chemistry. Part I. Methane and related
793 compounds. *J. Phys. Chem. Ref. Data* 1986;15:1087–1280.
794
- 795 [65] Baulch DL, Bowman CT, Cobos CJ, Cox RA, Just T, Kerr JA, Pilling MJ, Stocker D, Troe J, Tsang W,
796 Walker RW, Warnatz J. Evaluated kinetic data for combustion modeling: Supplement II. *J. Phys. Chem. Ref.*
797 *Data* 2005;34:757–1397.
798
- 799 [66] Ellingson BA, Theis DP, Tishchenko O, Zheng J, Truhlar DG. Reactions of hydrogen atom with hydrogen
800 peroxide. *J. Phys. Chem. A* 2007;111:13554–13566.
801
- 802 [67] Mittal G, Sung CJ, Yetter RA. Autoignition of H_2/CO at elevated pressures in a rapid compression
803 machine. *Int J Chem Kinet* 2006;38:516-529.
804
- 805 [68] Zhao ZW, Li J, Kazakov A, Dryer FL. Temperature-dependent feature sensitivity analysis for combustion
806 modelling. *Int. J. Chem. Kinet.* 2005;37:282–295.
807
- 808 [69] Cohen N. Are reaction rate coefficients additive? Revised transition state theory calculations for $OH +$
809 alkane reactions. *Int J Chem. Kinet* 1991;23:397-417.
810
- 811 [70] Baulch DL, Cobos CJ, Cox RA, Frank P, Hayman G, Just Th, Kerr JA, Murrells T, Pilling MJ, Troe J,
812 Walker RW, Warnatz J. Evaluated kinetic data for combustion modeling. Supplement I. *J Phys Chem Ref Data*
813 1994;23:847.
814
- 815 [71] Madronich S, Felder W. Direct measurements of the rate coefficient for the reaction $OH+CH_4 \rightarrow$
816 CH_3+H_2O over 300-1500 K. *Proc Comb Inst* 1984;20:703-713.
817
- 818 [72] Srinivasan NK, Su MC, Sutherland W. Reflected Shock Tube Studies of High-Temperature Rate

819 Constants for $\text{OH}+\text{CH}_4\rightarrow\text{CH}_3+\text{H}_2\text{O}$ and $\text{CH}_3+\text{NO}_2\rightarrow\text{CH}_3\text{O}+\text{NO}$. *J Phys Chem A* 2005;109:1857-1863.
820
821 [73] Li SC, Williams FA. Reaction mechanisms for methane ignition. *J Engr Gas Turb Power*
822 2002;124:471-480.
823
824 [74] Aul, CJ, Metcalfe WK, Burke SM, Curran HJ, Petersen EL. Ignition and kinetic modeling of methane and
825 ethane fuel blends with oxygen: A design of experiments approach. *Comb and Flame* 2013;160:1153-1167.
826
827 [75] Chemical-Kinetic Mechanisms for Combustion Applications, Mechanical and Aerospace Engineering
828 (Combustion Research), University of California at San Diego 2011.
829
830 [76] Srinivasan NK, Su MC, Sutherland JW, Michael JV. Reflected shock tube studies of high-temperature rate
831 constants for CH_3+O_2 , $\text{H}_2\text{CO}+\text{O}_2$, and $\text{OH}+\text{O}_2$. *J. Phys. Chem. A* 2005;109:7902–7914.
832
833 [77] Herbon JT, Hanson RK, Bowman CT, Golden DM. The reaction of CH_3+O_2 : experimental determination
834 of the rate coefficients for the product channels at high temperatures. *Proc Combust Inst* 2005;30:955–963.
835
836 [78] Baulch DL, Cobos CJ, Cox RA, Frank P, Hayman G, Just T, Kerr JA, Murrells T, Pilling MJ, Troe J,
837 Walker RW, Warnatz J. Summary table of evaluated kinetic data for combustion modeling: Supplement 1.
838 *Combust Flame* 1994;98:59–79.
839
840 [79] Sutherland JW, Michael JV, Pirraglia AN, Nesbitt FL, Klemm RB. Rate constant for the reaction of $\text{O}(^3\text{P})$
841 with H_2 by the flash photolysis-shock tube and flash photolysis-resonance fluorescence techniques;
842 $504\text{K}\leq T\leq 2495\text{K}$. *Proc Combust Inst* 1988;21:929–941.
843
844 [80] Natarajan K, Roth P. High temperature rate coefficient for the reaction of $\text{O}(^3\text{P})$ with H_2 obtained by the
845 resonance absorption of O and H atoms. *Combust Flame* 1987;70:267–279.
846
847 [81] Davidson DF, Hanson RK. A direct comparison of shock tube photolysis and pyrolysis methods in the
848 determination of the rate coefficient for $\text{O} + \text{H}_2\rightarrow \text{OH} + \text{H}$. *Combust Flame* 1990;82:445–447.
849
850 [82] Javoy S, Naudet V, Abid S, Paillard CE. Rate constant for the reaction of O with H_2 at high temperature
851 by resonance absorption measurements of O atoms. *Int J Chem Kinet* 2000;32:686–695.
852
853 [83] Smith IWM, Crim FF. The chemical kinetics and dynamics of the prototypical reaction: $\text{OH} + \text{H}_2\rightarrow \text{H}_2\text{O}$
854 $+ \text{H}$. *Phys Chem Chem Phys* 2002;4:3543–3551.
855
856 [84] Konnov AA. *Khim Fiz* 2004;23:5–18.
857
858 [85] Konnov AA. Detailed reaction mechanism for small hydrocarbons combustion, Release 0.5, 2000.
859
860 [86] Krasnoperov LN, Michael JV. Shock tube studies using a novel multipass absorption cell: rate constant
861 results for $\text{OH} + \text{H}_2$ and $\text{OH} + \text{C}_2\text{H}_6$. *J Phys Chem A* 2004;108:5643–5648.
862
863 [87] Oldenberg RC, Loge GW, Harradine DM, Winn KR. Kinetic study of the hydrogel + hydrogen reaction
864 from 800 to 1550 K. *J Phys Chem* 1992;96:8426–8430.
865
866 [88] Law CK. *Combustion Physics*. Cambridge University Press 2006.

866 [89] Kim TJ, Yetter RA, Dryer FL. New results on CO oxidation: High pressure, high temperature experiments
867 and comprehensive kinetic modeling. Proc Combust Inst 1994;25:759-766.

868 [90] Lindstedt RP, Skevis G. Chemistry of acetylene flames. Combust Sci Technol 1997;125:73-137.

869 [91] Li J, Zhao Zh, Kazakov A, Dryer FL. An updated comprehensive kinetic model of hydrogen combustion.
870 Int J Chem Kinet 2004;36:566-575.

871 [92] Burke MP, Chaos M, Ju Y, Dryer FL, Klippenstein SJ. Comprehensive H₂/O₂ kinetic model for
872 high-pressure combustion. Int. J Chem Kinet 2012;44:444-474.

873 [93] Hong ZK, Vasu SS, Davidson DF, Hanson RK. Experimental study of the rate of OH + HO₂ --> H₂O +
874 O₂ at high temperatures using the reverse reaction. J Phys Chem A 2010;114:5520-5525.

875 [94] Hu E, Fu J, Pan L, Jiang X, Huang Z, Zhang Y. Experimental and numerical study on the effect of
876 composition on laminar burning velocities of H₂/CO/N₂/CO₂/air mixtures. Int J Hydrogen Energy
877 2012;37:18509-18519.

878 [95] Davis SG, Joshi AV, Wang H, Egolfopoulos F. An optimized kinetic model of H₂/CO combustion. Proc
879 Combust Inst 2005;30:1283-1292.

880

881 [96] O'Conaire M, Curran HJ, Simmie JM, Pitz WJ, Westbrook CK. A comprehensive modeling study of
882 hydrogen oxidation. Int J Chem Kinet 2004;36:603-622.

883

884 [97] Mallard WG, Westley F, Herron JT, Hanson RF. NIST Standard Reference Database 17 2Q98; NIST
885 Standard Reference Data: Gaithersburg, MD, 1994.

886

887 [98] Hippler H, Troe J, Willner J. Shock wave study of the reaction HO₂ + HO₂ = H₂O₂ + O₂: Confirmation
888 of a rate constant minimum near 700 K. J. Chem. Phys 1990;93:1755-1760.

889

890

891

892

893

894

895

896

897

898

899

900

901

902

903

904

905

906

907

908

909

FIGURE CAPTIONS

910

911

912 Figure 1. The 13 most sensitive reactions for syngas type 1 at 1000K and pressures 10, 30 and 50 bar.

913

914 Figure 2. Comparison of ignition delay time for syngas types 1-4 obtained with new mechanism.

915

916 Figure 3. Comparison of ignition delay time for syngas type 1 obtained with new mechanism with other
917 mechanisms at temperatures 800-1052K, pressures 20, 40, 80 bars and equivalence ratio 0.6.

918

919 Figure 4. Comparison of ignition delay time for syngas type 4 obtained with new mechanism with other
920 mechanisms at temperatures 800-1052K, pressures 20, 40, 80 bars and equivalence ratio 0.6.

921

922 Figure 5. Effect of CO concentration on ignition delay times of syngas mixtures compared with Keromnes
923 et al. [35] mechanism.

924

925 Figure 6. Laminar flame speed results obtained with new mechanism for syngas types 1-4 and compared
926 with other mechanisms.

927

928 Figure 7. Laminar flame speed of $H_2/CO/CO_2$ -35:35:30 fuel mixture at $P=1-3$ atm and $T=303-373$ K.

929

930 Figure 8. Calculated laminar flame speed of H_2/CH_4 fuel mixture obtained with new mechanism at
931 $P=1$ atm and $T=298$ K and compared with different kinetic models.

932

933 Figure 9. Effect of pressure on the laminar flame speed obtained with new mechanism for syngas type 1 and
934 comparison with different kinetic mechanisms.

935

936 Figure 10. Comparison of CFD in-cylinder pressure obtained using the new mechanism with the results
937 using different chemical kinetics mechanisms for syngas types 1-3, equivalence ratio 0.48, 0.52, 0.6 and
938 different timings of fuel micropilot injection.

939

940 Figure 11. The most sensitive reaction for modified syngas mechanism at temperature 1000K and
941 pressures 10, 30 and 50 bar.

942

943 Figure 12. Comparison of reaction flows of carbon atoms for syngas Type 1 and Type 4 at 30 bar. Flow values
944 are given in $mol/(cm^3 \text{ sec})$

945

946 Figure 13. Comparison of reaction flows of hydrogen atoms for syngas at temperature 1000 K and pressures 10,
947 30 and 50 bar. (A) type 1, (B) type 4. Fluxes below 1% of maximum flow have been filtered. Flow values are
948 given in $mol/(cm^3 \text{ sec})$

949

950 Figure 14. Data obtained with modified mechanism for syngas type 4 with high H_2 and compared with
951 other kinetic mechanisms. (A) Ignition delay calculated at temperatures 800-1052K, pressure 225kPa and
952 equivalence ratio 0.6. (B) Laminar flame speed calculated at temperature 450K, pressure 225K and
953 equivalence ratio 0.4-1.0.

954

955 Figure 15. Effect of different reaction rates of $H_2O_2+H=H_2+HO_2$ reaction on 3D CFD in-cylinder pressure
956 during micro-pilot ignited syngas combustion.

957
958
959
960
961
962
963
964
965
966
967
968
969
970
971
972
973
974
975
976
977
978
979
980
981
982
983
984
985
986
987
988
989
990
991
992
993
994
995
996
997
998
999
1000
1001
1002
1003

Figure 16. Comparison of experimental and simulated in-cylinder pressures and heat release rates of dual-fuel micro-pilot ignited syngas combustion. Computed using 3D-CFD with new kinetic mechanism. (A-B) Type 1, (C-D) Type 2, (E-F) Type 3 and (G-H) Type 4. $P_{IVC} = 225$ kPa, $T_{IVC} = 330$ K.

Figure 17. Sequential images of dual-fuel micro-pilot ignited syngas combustion with new kinetics mechanisms. (A) New mechanism, Type 3, $\phi=0.6$, $\theta_{inj} = 14^{\circ}$ BTDC, $P_{IVC} = 225$ kPa, $T_{IVC} = 330$ K. (B) Modified mechanism, Type 4, $\phi=0.6$, $\theta_{inj} = 3^{\circ}$ BTDC, $P_{IVC} = 225$ kPa, $T_{IVC} = 330$ K.

1004

TABLE CAPTIONS

1005

1006 Table 1. Engine specification and simulation conditions

1007 Table 2. Syngas composition

1008 Table 3. Chemical kinetics mechanism for micro pilot-ignited dual-fuel syngas combustion simulation (A units
1009 cal-cm-sec-K, E units cal/mol).

1010 Table 4. Mixture composition of the ignition delay times experiments in the RCM from the University of
1011 Connecticut.

1012

1013

SUPPLEMENTARY DATA

1014

1015 Animation file 1. Diesel micro-pilot ignited dual-fuel combustion of syngas. Top View, Type 3,
1016 $\phi=0.6$.

1017

1018 Animation file 2. Diesel micro-pilot ignited dual-fuel combustion of syngas. Side View, Type 3,
1019 $\phi=0.6$.

1020

1021 Animation file 3. Diesel micro-pilot ignited dual-fuel combustion of syngas. Top View, Type 6,
1022 $\phi=0.6$.

1023

1024 Animation file 4. Diesel micro-pilot ignited dual-fuel combustion of syngas. Side View Type 6,
1025 $\phi=0.6$.

1026

Table 1

[Click here to download high resolution image](#)

Engine type	4-stroke, single cylinder water cooled
Bore x Stroke	96 x 108 mm
Swept volume	781.7 cm ³
Compression ratio	16
Combustion system	Dual-fuel, direct injection
Combustion chamber	Shallow dish
Engine speed	1000 rpm
Intake valve closure (IVC)	135 deg. BTDC
Initial pressure at IVC	225 kPa
Initial temperature at IVC	330 K
Injection system	Common-rail
Nozzle hole x diameter	4x0.10 mm
Pilot fuel injection pressure	80 MPa
Pilot fuel injection quantity	1.2 mg/cycle
Equivalence ratio	Variable

Table 2

[Click here to download high resolution image](#)

Gas type	Composition					LHV (MJ/kg)	Source
	H ₂ (%)	CO (%)	CH ₄ (%)	CO ₂ (%)	N ₂ (%)		
Type 1	13.7	22.3	1.9	16.8	45.3	4.13	BMG
Type 2	20.0	22.3	1.9	16.8	39.0	4.99	BMG
Type 3	13.7	22.3	1.9	23.0	39.1	3.98	BMG
Type 4	56.8	5.9	29.5	2.2	5.6	38.69	COG

Table 3

[Click here to download high resolution image](#)

Skeletal syngas mechanism

	Reactions	A	n	E _A	Ref.
R1	C7H16+11O2=7CO2+8H2O /EBU/ 4. 0. 1 0.	0.	0.	0.	[47]
R2	CH4+O2=CH3+HO2	3.98E13	0.0	56855.5	[46]
R3	CH4+HO2=CH3+H2O2	0.964E11	0.0	24629.4	[46]
R4	CH4+OH=CH3+H2O	1.60E07	1.83	2771.1	[73]
R5	CH3+O2=CH2O+OH	3.30E11	0.0	8934.4	[25]
R6	CH2O+OH=HCO+H2O	3.90E10	0.0	406.1	[46]
R7	CO+O(+M)=CO2(+M) /LOW / 0.2070E27 -3.340 7610.0 /M/ H2O/12.00/ H2/2.00/ CO/1.50/ CO2/2.00/ AR/0.50/	9.04E12	0.89	3800.0	[25]
R8	CO+OH=CO2+H	0.9600E12	0.14	7352.0	[25]
R9	CO+OH=CO2+H	0.7320E11	-1.00	-16.0	[25]
R10	CO+HO2=CO2+OH	0.1200E18	0.00	17000.0	[25]
R11	CO+H2O=CO2+H2	0.2000E9	0.00	38000.0	[25]
R12	HCO(+M)=CO+H(+M) /M/ H2O/5.00/ CO2/3.00/ H2/1.90/ CO/1.90/	0.3000E14	0.03	23000.0	[25]
R13	HCO+O=CO2+H	0.3000E14	0.00	0.0	[25]
R14	HCO+H=H2+CO	0.1000E13	0.00	0.0	[25]
R15	HCO+OH=H2O+CO	0.5000E14	0.00	0.0	[25]
R16	HCO+HO2=H2O2+CO	0.4000E12	0.00	0.0	[25]
R17	HCO+HO2=>H+OH+CO2	0.3000E14	0.00	0.0	[25]
R18	O2+CO=CO2+O	0.2530E10	0.00	0.0	[25]
R19	O2+HCO=HO2+CO	0.1000E15	0.00	47700.0	[25]
R20	OH+OH(+M)=H2O2(+M) /LOW / 0.2300E19 -0.900 -1700.0 /TROE/ 0.7346 94.00 1756.0 5182.0 /M/ H2/3.00 /H2O/6.00/ CO/1.50/ CO2/2.00/ AR/0.70/	0.7400E14	-0.370	0.0	[25]
R21	H+O2=OH+O	3.52E16	-0.7	17061.4	[63]
R22	H2+O=OH+H	5.06E4	2.67	6287.6	[79]
R23	H2+OH=H2O+H	1.17E9	1.3	0.0	[79]
R24	H+O2(+M)=>HO2(+M) /LOW / 1.737E19 -1.23 0.0 /M/ AR/0.0/ H2/1.3/ H2O/10.0/ CO/1.9/ CO2/3.8/	4.6E12	0.4	0.0	[35]
R25	H+H(+M)=>H2(+M) /M/ H2/2.5/ H2O/12.0/ CO/1.9 /CO2/3.8/ AR/0.5/	1.30E18	-1	0.0	[63]
R26	H+OH(+M)=>H2O(+M) /M/ H2/2.5/ H2O/12.0/ CO/1.9/ CO2/3.8/ AR/0.38/	4.00E22	-2	0.0	[63]
R27	HO2+H=>OH+OH	7.08E13	0.0	298.8	[97]
R28	HO2+H=H2+O2	1.66E13	0.0	821.8	[35]
R29	HO2+OH=H2O+O2	2.89E13	0.0	-500	[42]
R30	HO2+HO2=H2O2+O2	1.300E11	0.00	-1.630E03	[35]

Additional reactions for biomass feedstock derived gas (low H₂ concentration)

	Reactions	A	n	E _A	Ref.
R29b	HO2+OH=H2O+O2	2.456E13	0.0	-4.97E02	[35]
R31	H2O2+H=H2+HO2	7.7E12	0.0	3755	[42]
R32	O+H2O=OH+OH	2.97E06	2.02	1.340E04	[35]

Reaction constants for coke-oven feedstock derived gas (high H₂ concentration)

	Reactions	A	n	E _A	Ref.
R31	H2O2+H=H2+HO2	1.21E07	0.0	5200	[49]

Table 4

[Click here to download high resolution image](#)

H ₂ (%)	CO (%)	O ₂ (%)	N ₂ (%)	T_c (K)
12.500	0.000	6.250	81.250	914 -1010
6.250	6.250	6.250	81.250	929 -1031
3.125	9.375	6.250	81.250	959 -1052
1.250	11.250	6.250	81.250	973 -1068

Figure 1
[Click here to download high resolution image](#)

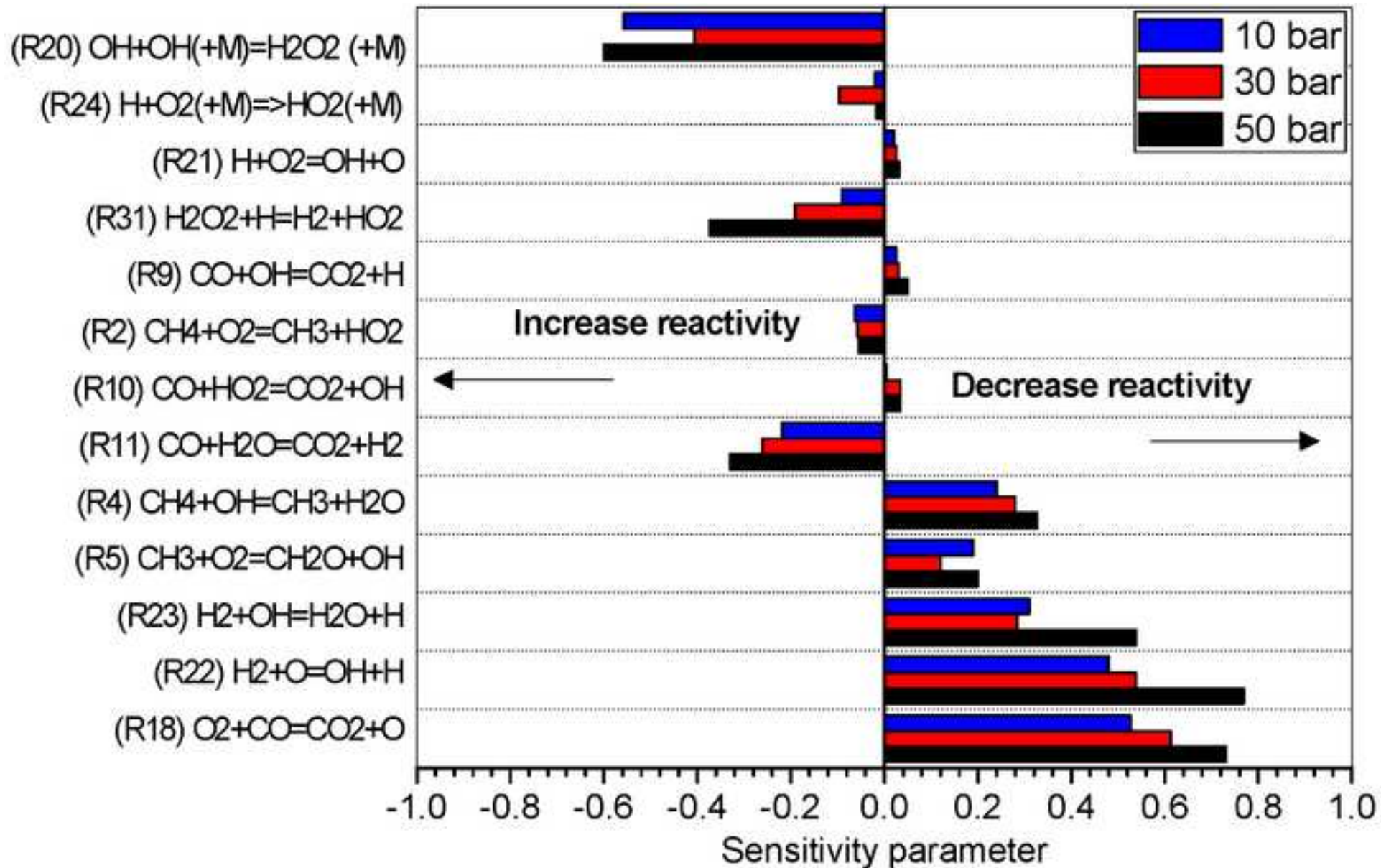


Figure 2
[Click here to download high resolution image](#)

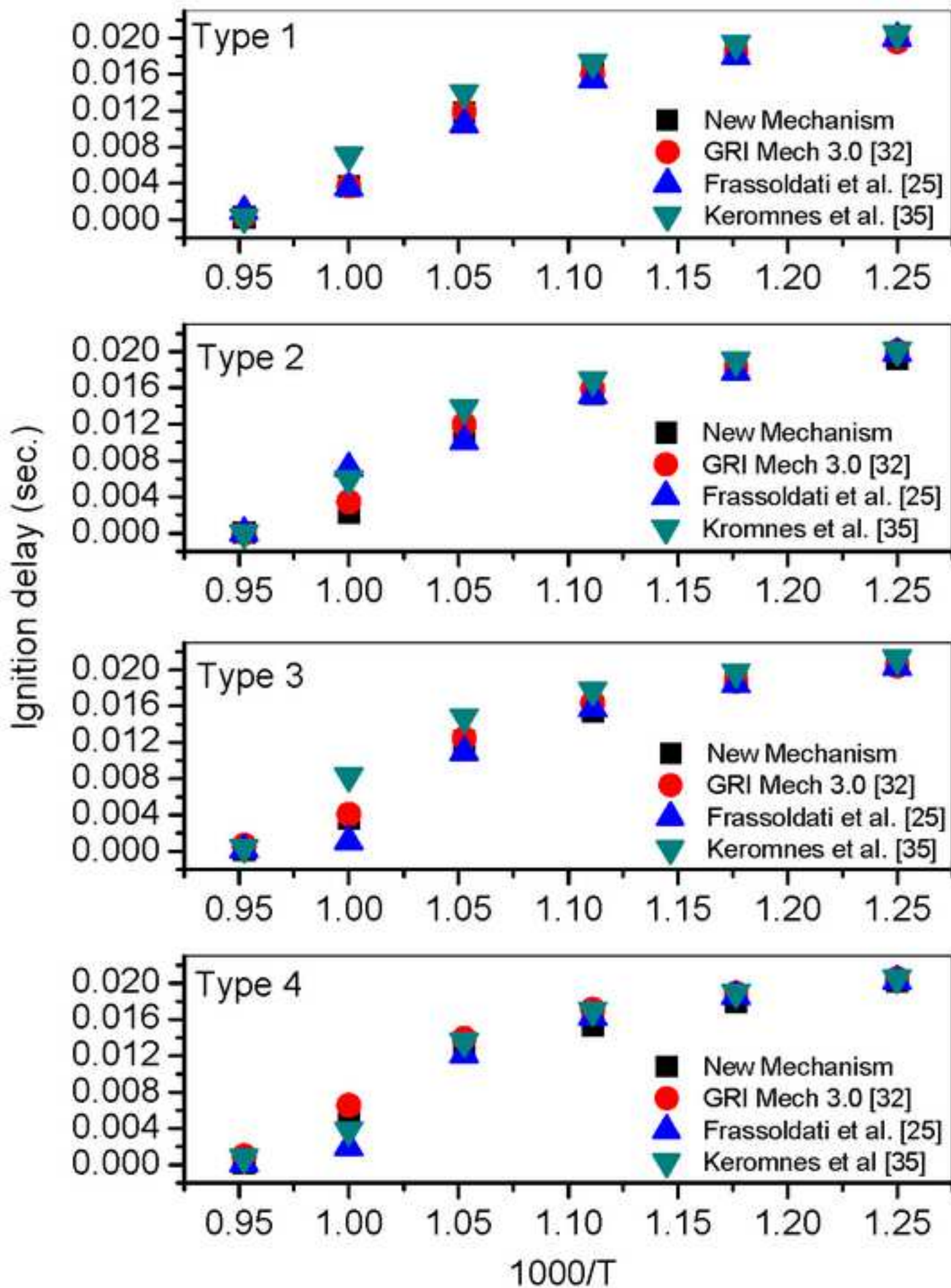


Figure 3
[Click here to download high resolution image](#)

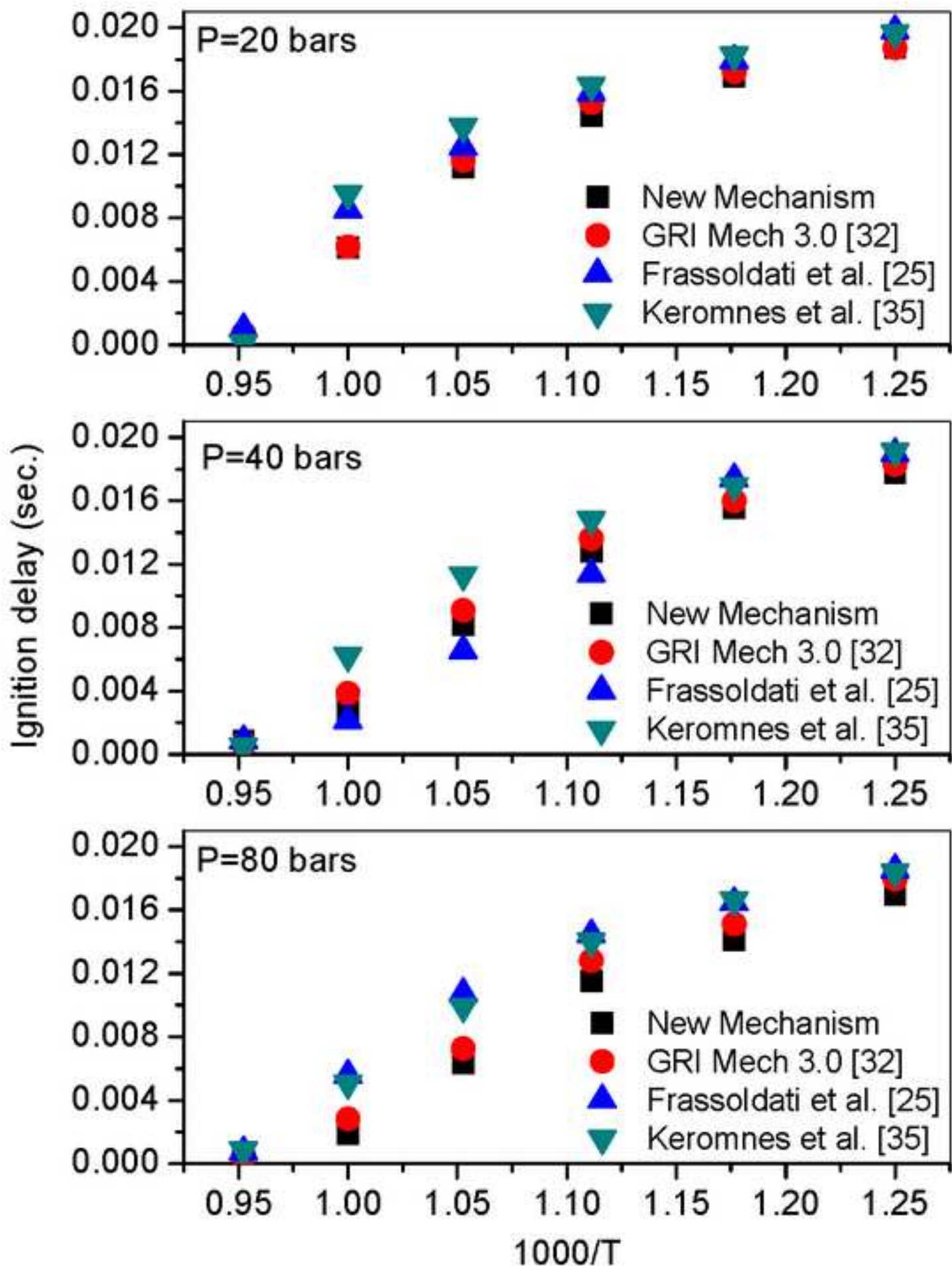


Figure 4

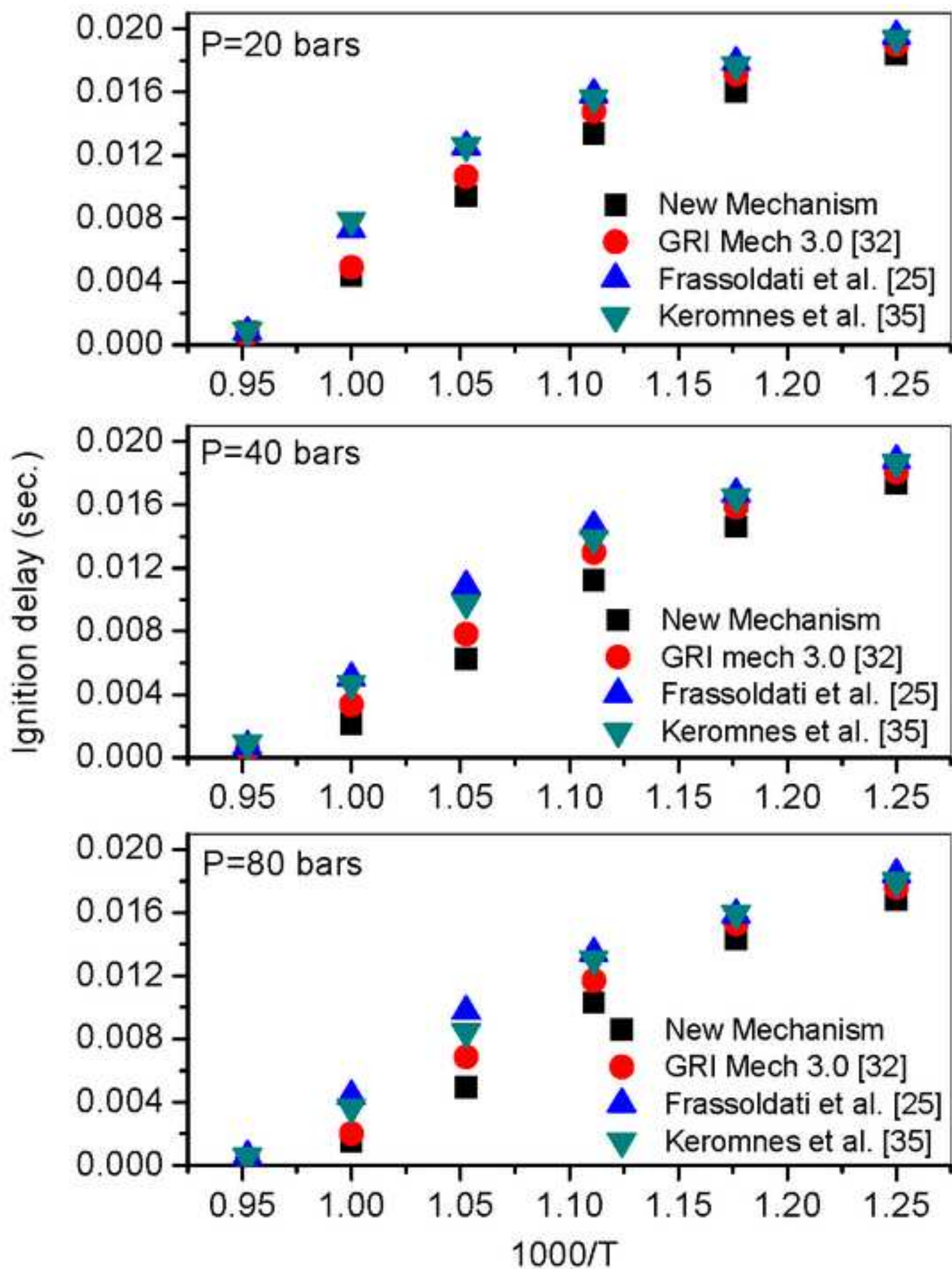
[Click here to download high resolution image](#)

Figure 5
[Click here to download high resolution image](#)

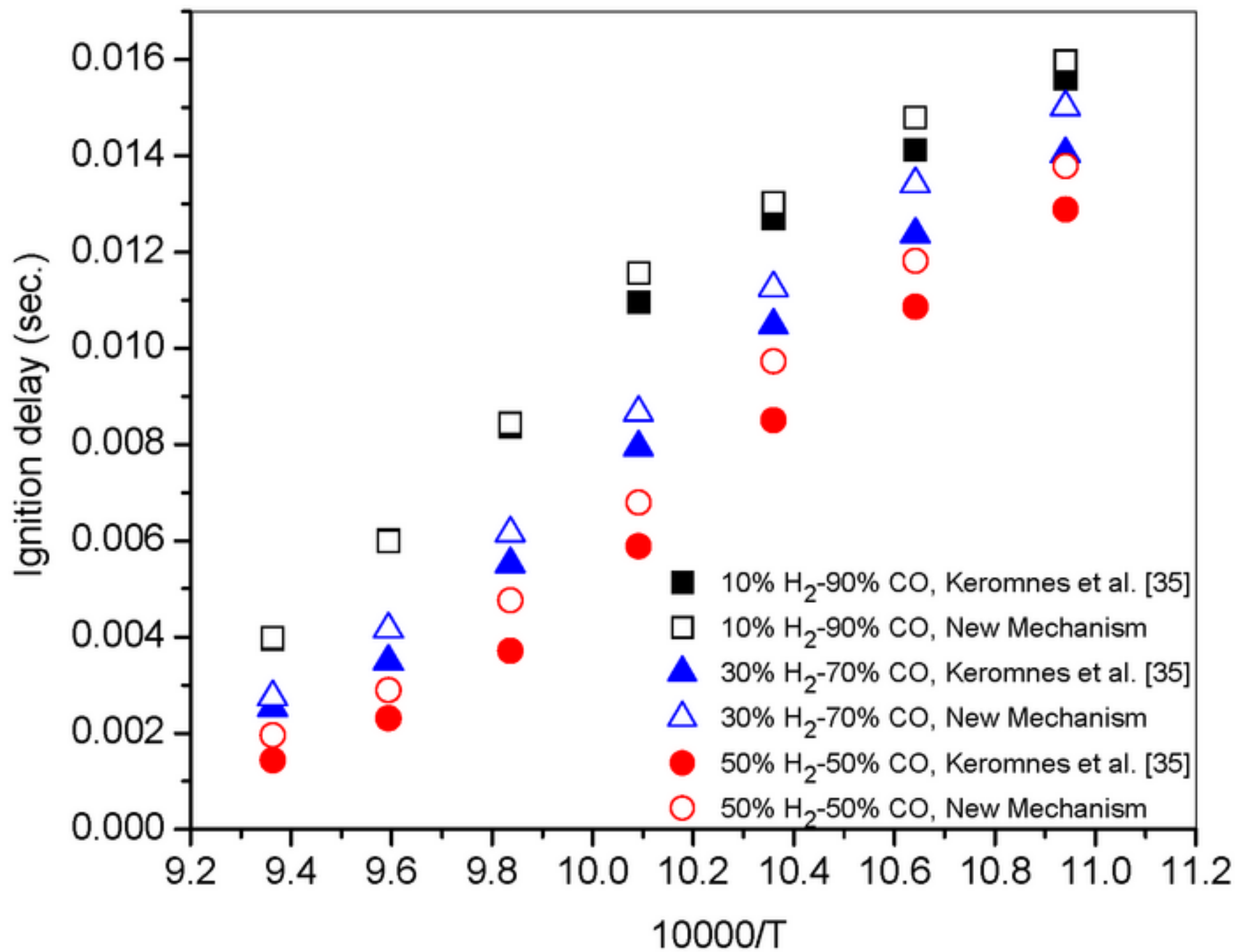


Figure 6

[Click here to download high resolution image](#)

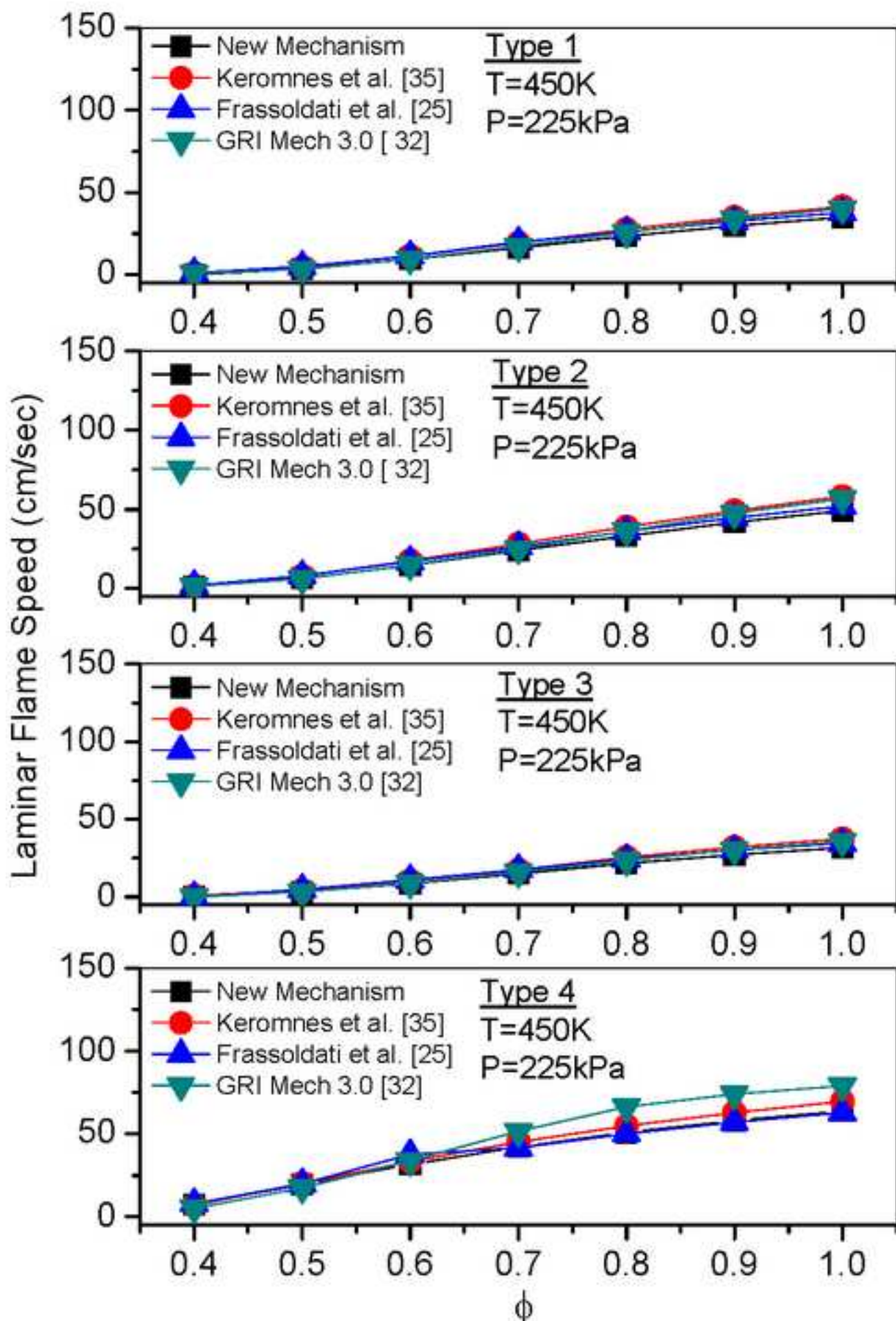


Figure 7

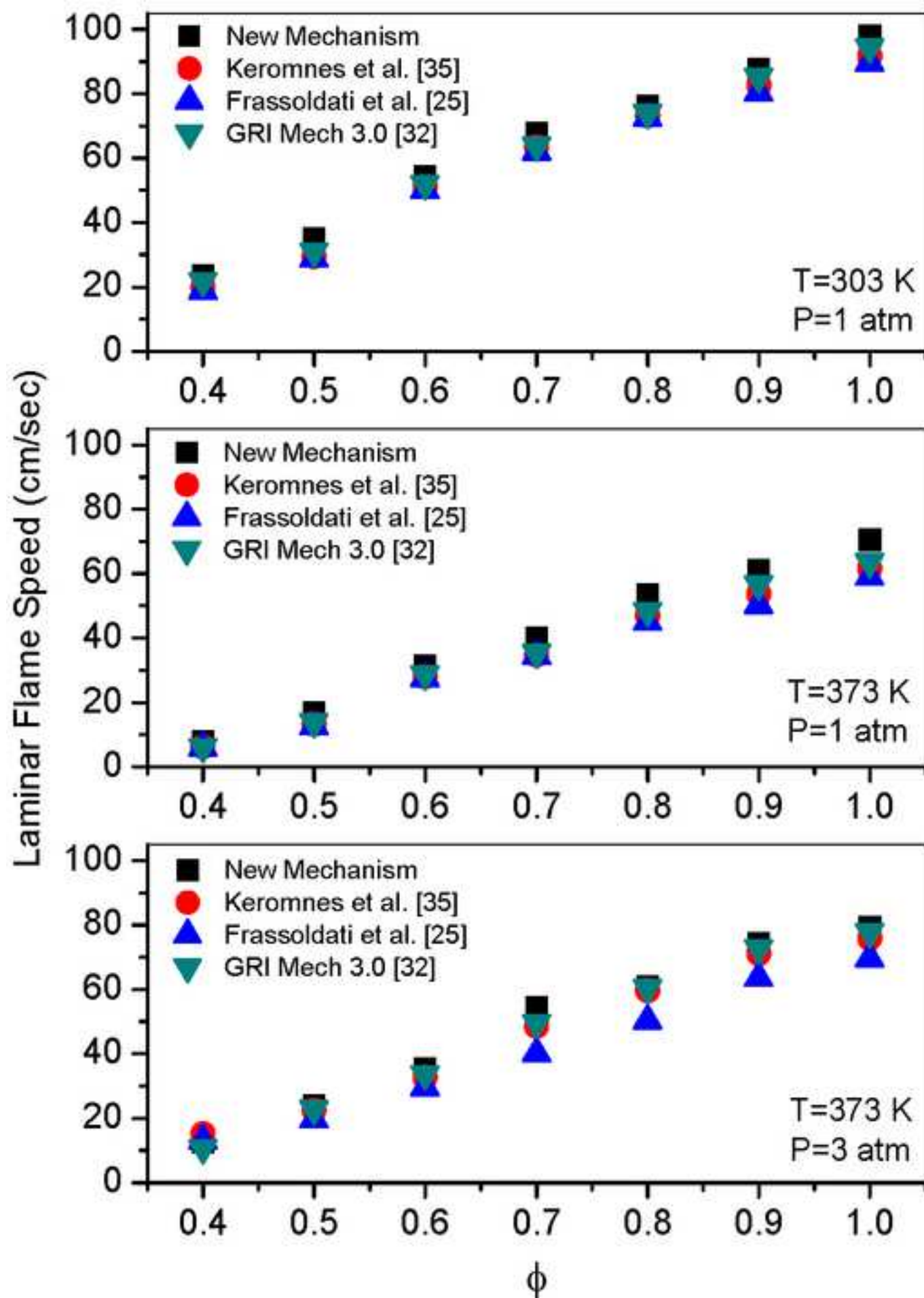
[Click here to download high resolution image](#)

Figure 8

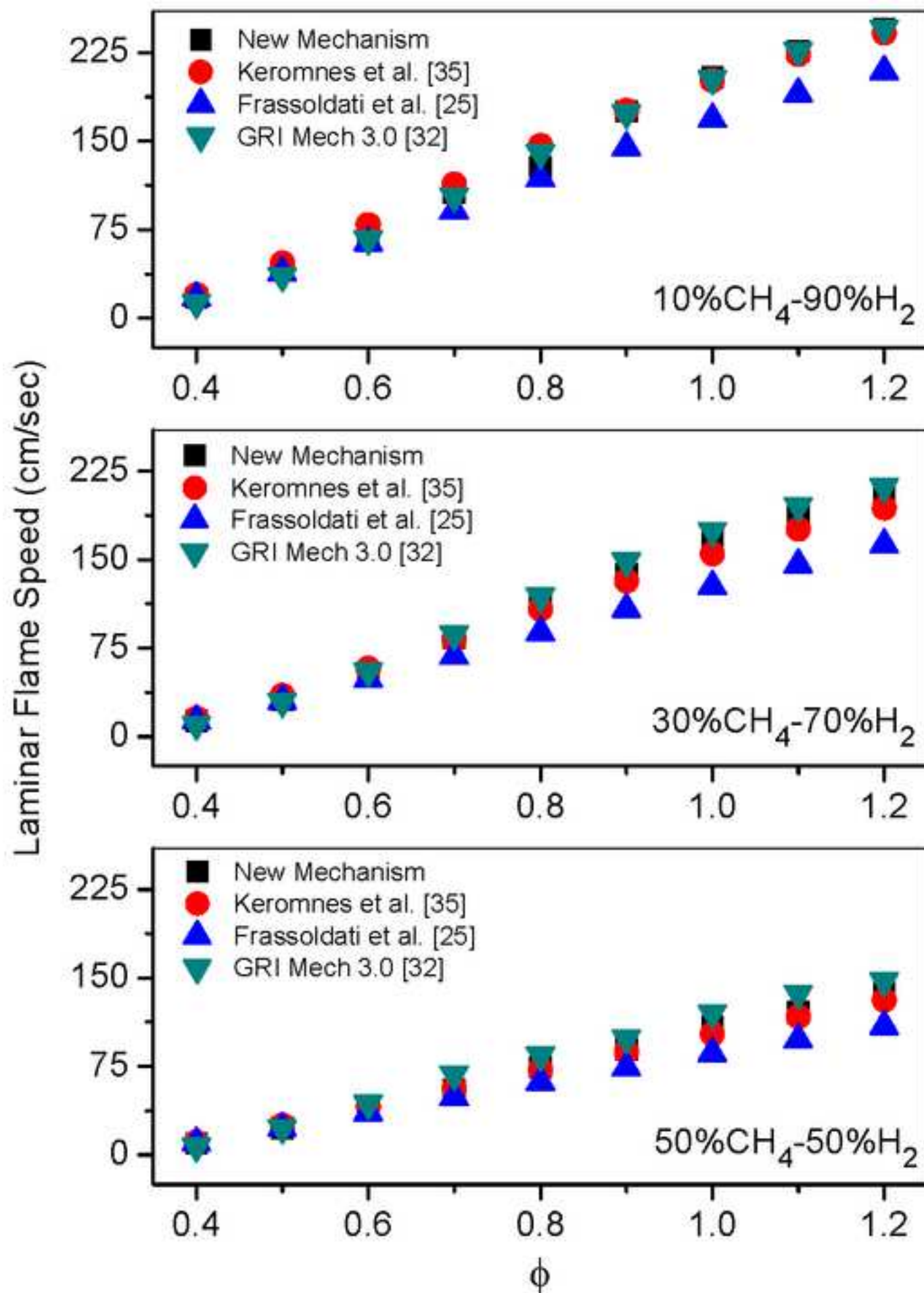
[Click here to download high resolution image](#)

Figure 9

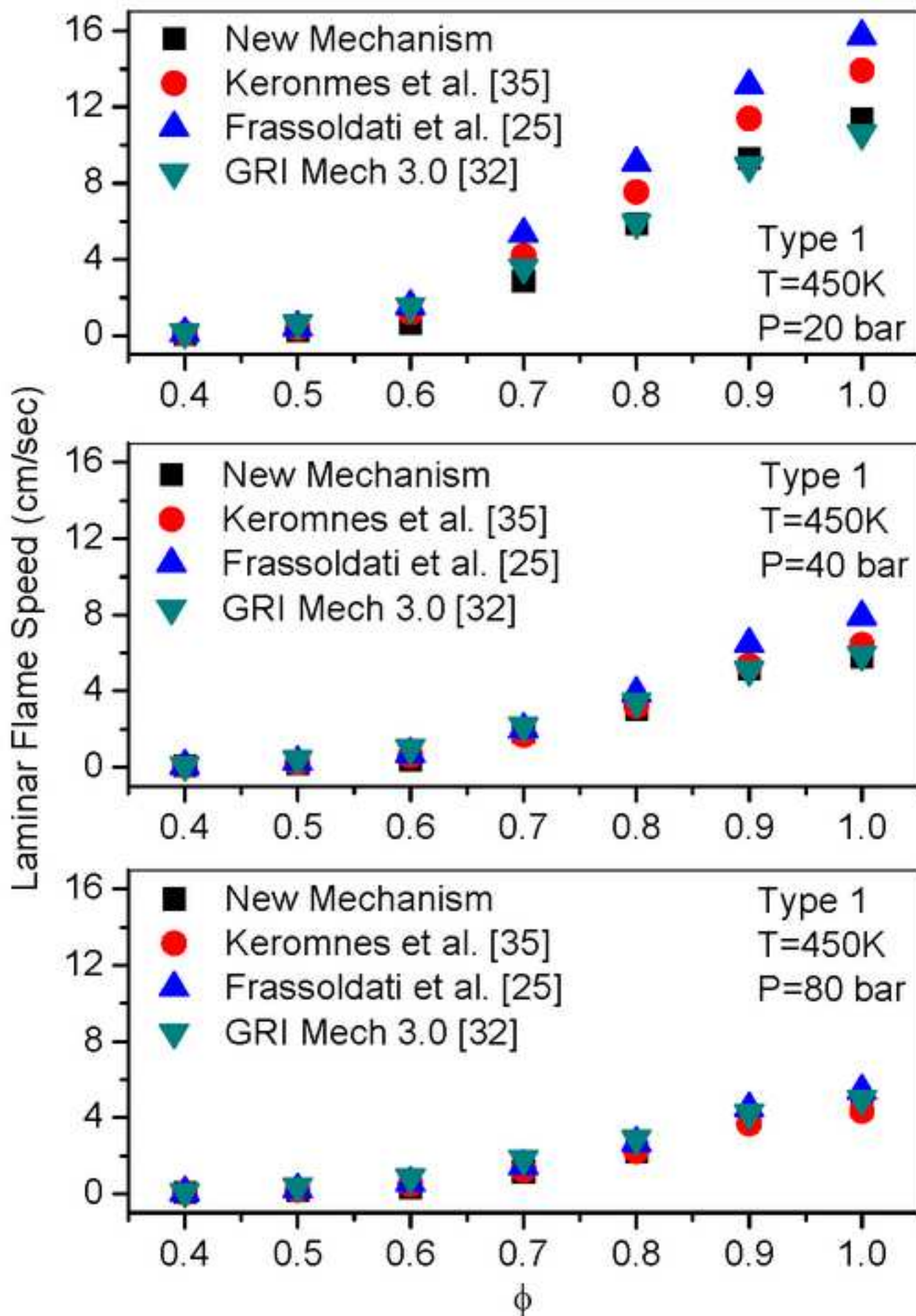
[Click here to download high resolution image](#)

Figure 10

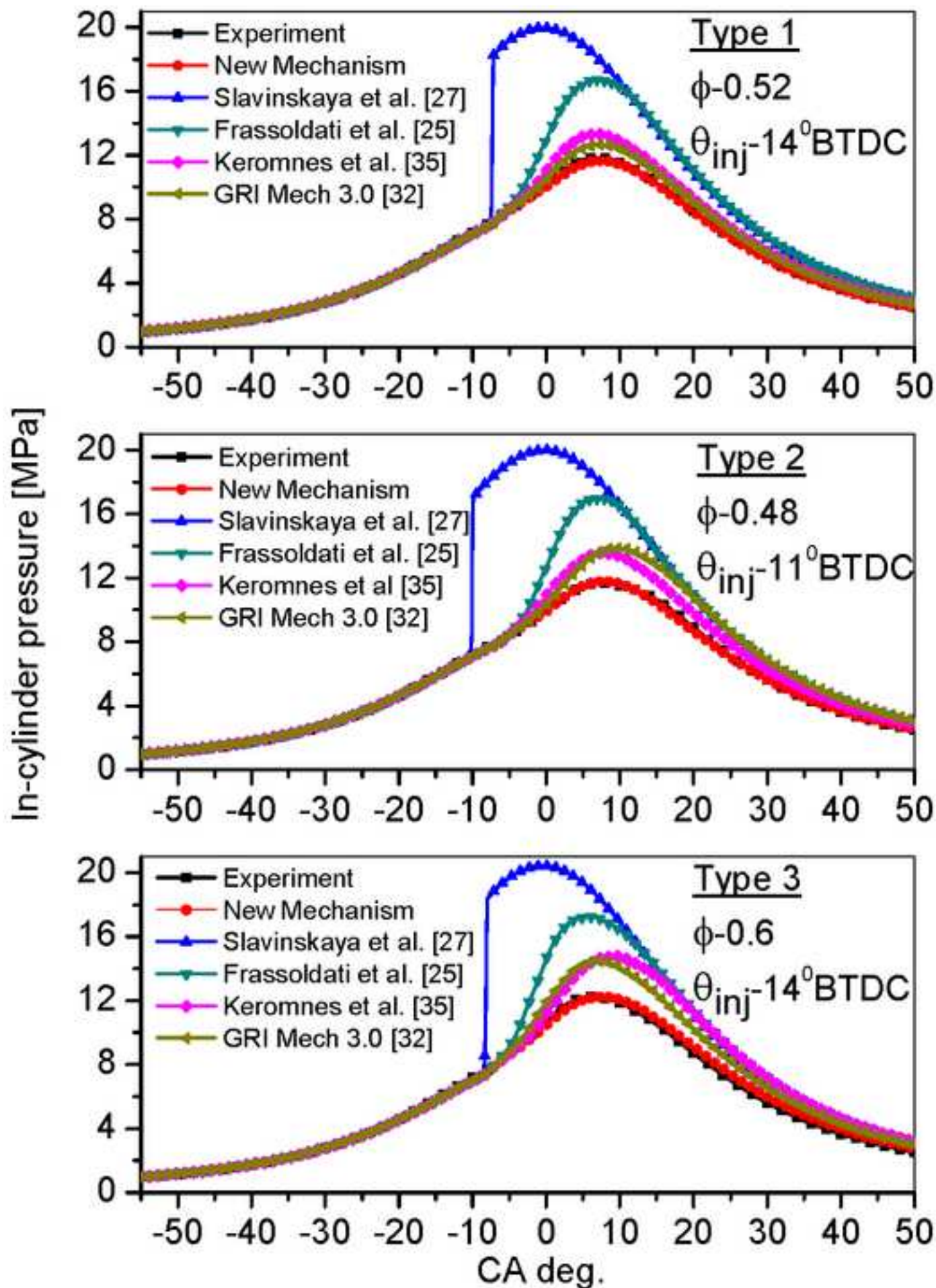
[Click here to download high resolution image](#)

Figure 11
[Click here to download high resolution image](#)

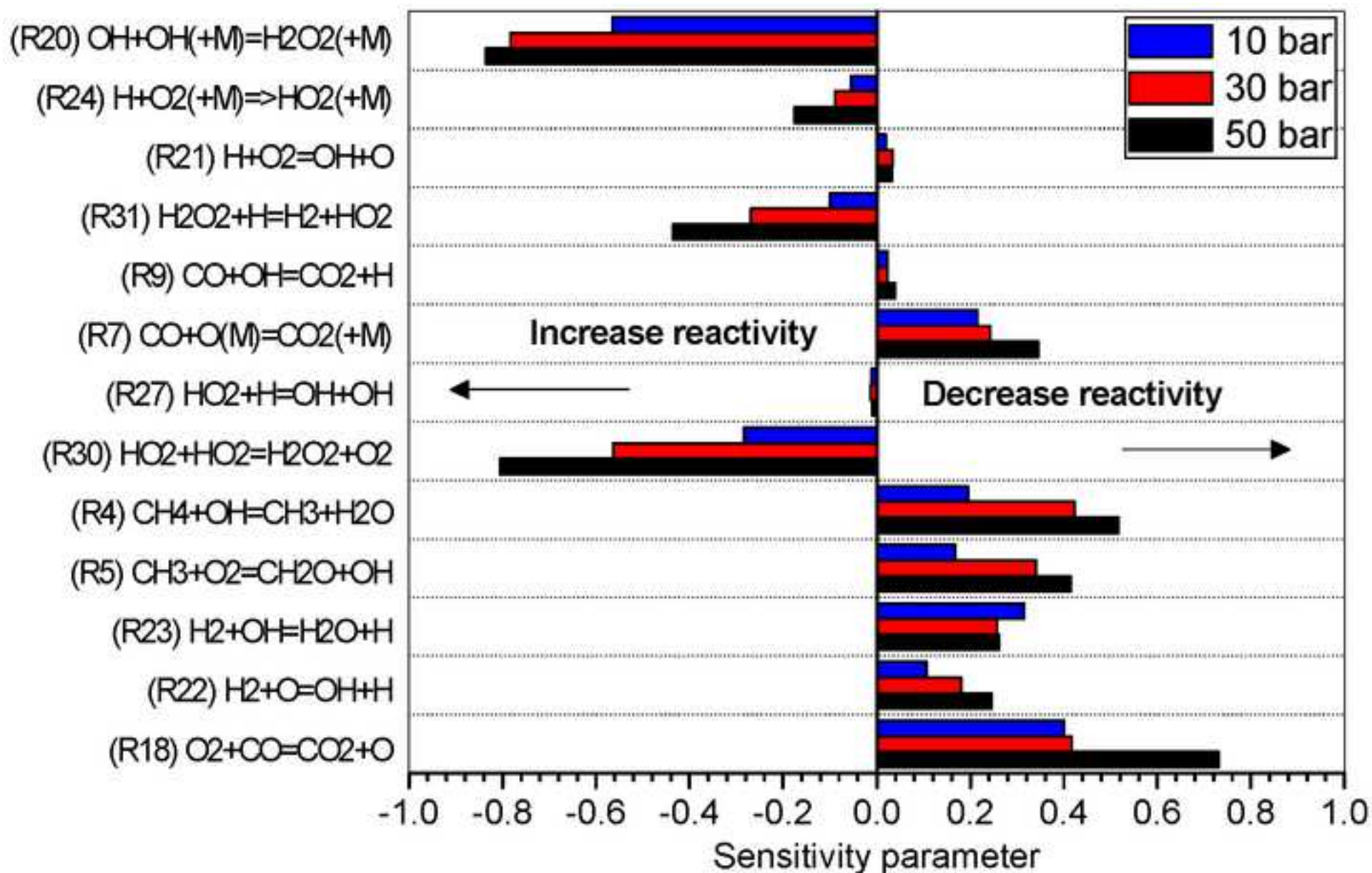
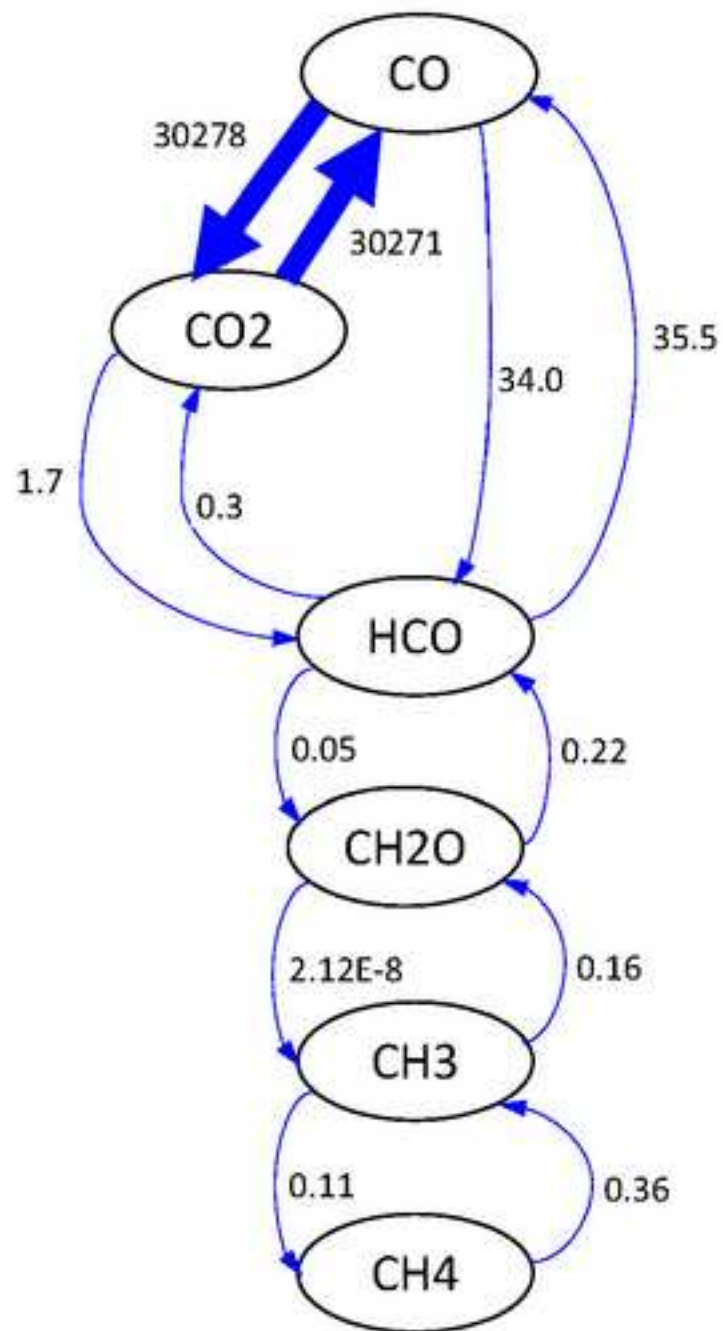


Figure 12

[Click here to download high resolution image](#)

Syngas Type 1



Syngas Type 4

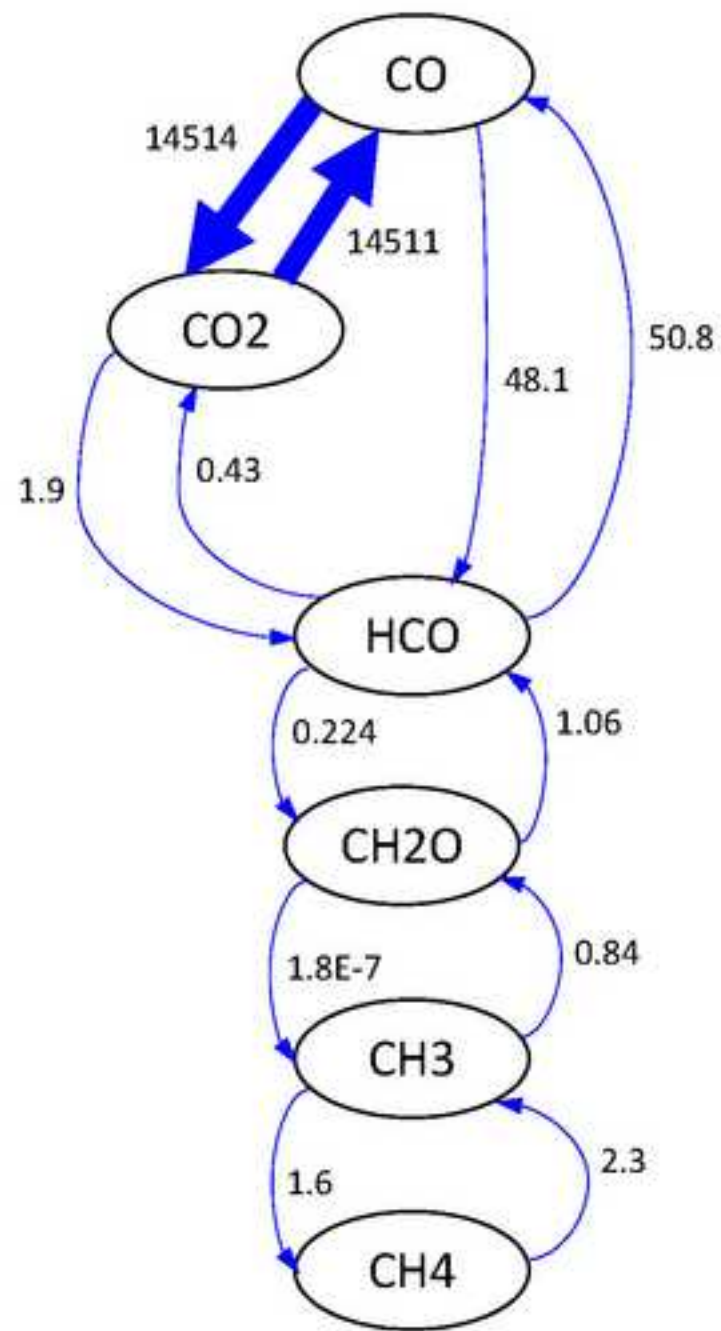


Figure 13
[Click here to download high resolution image](#)

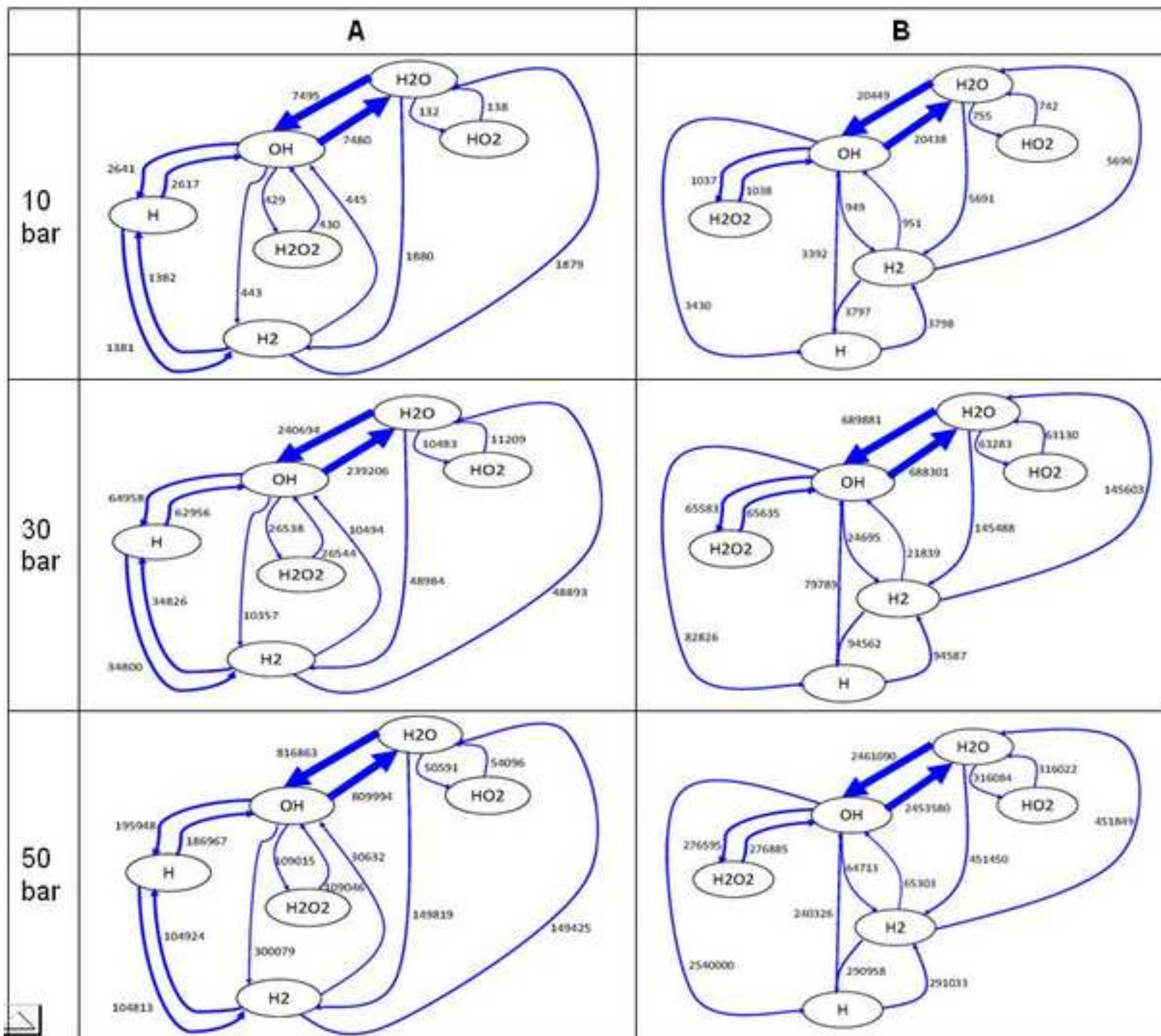


Figure 14

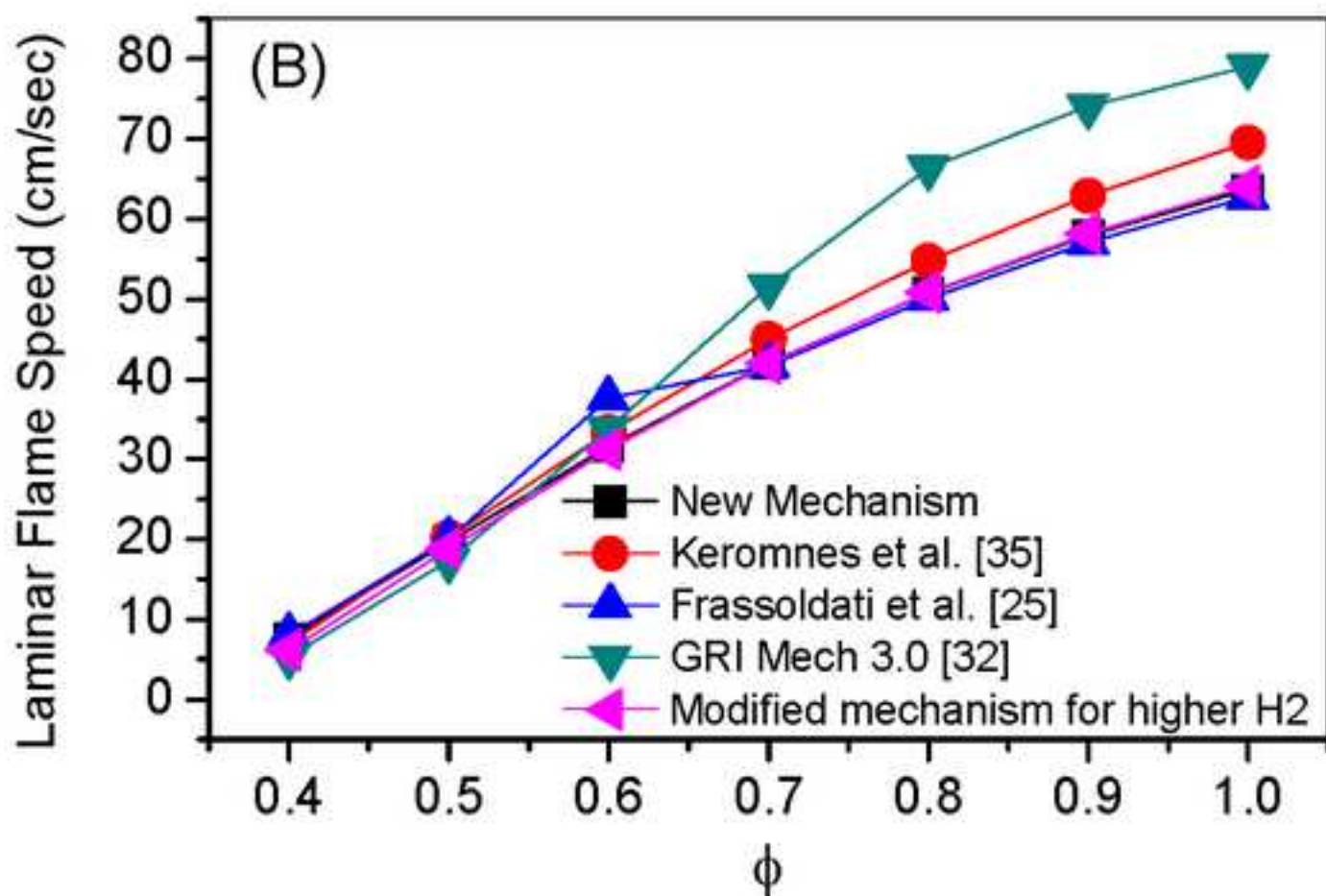
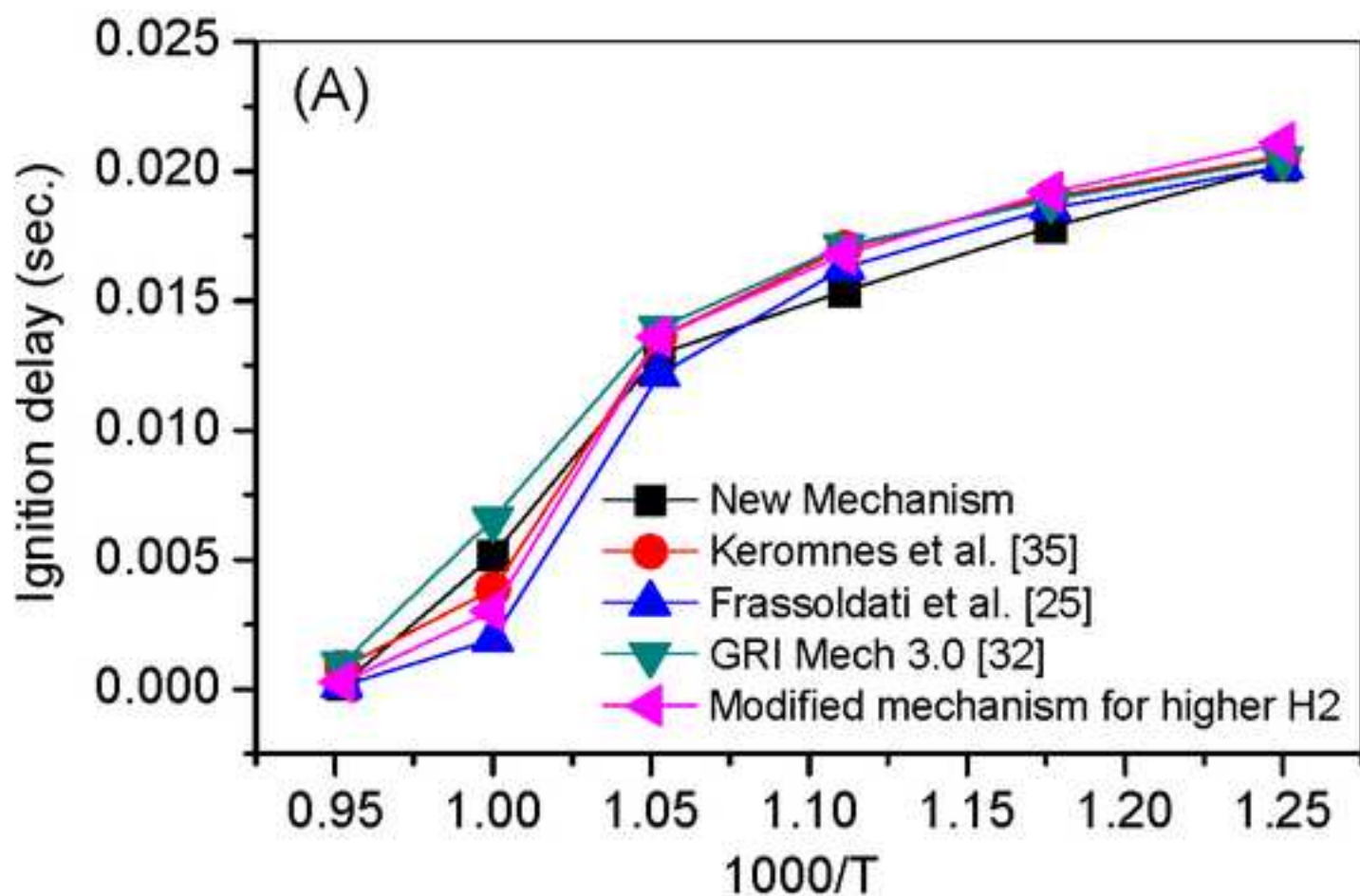
[Click here to download high resolution image](#)

Figure 15

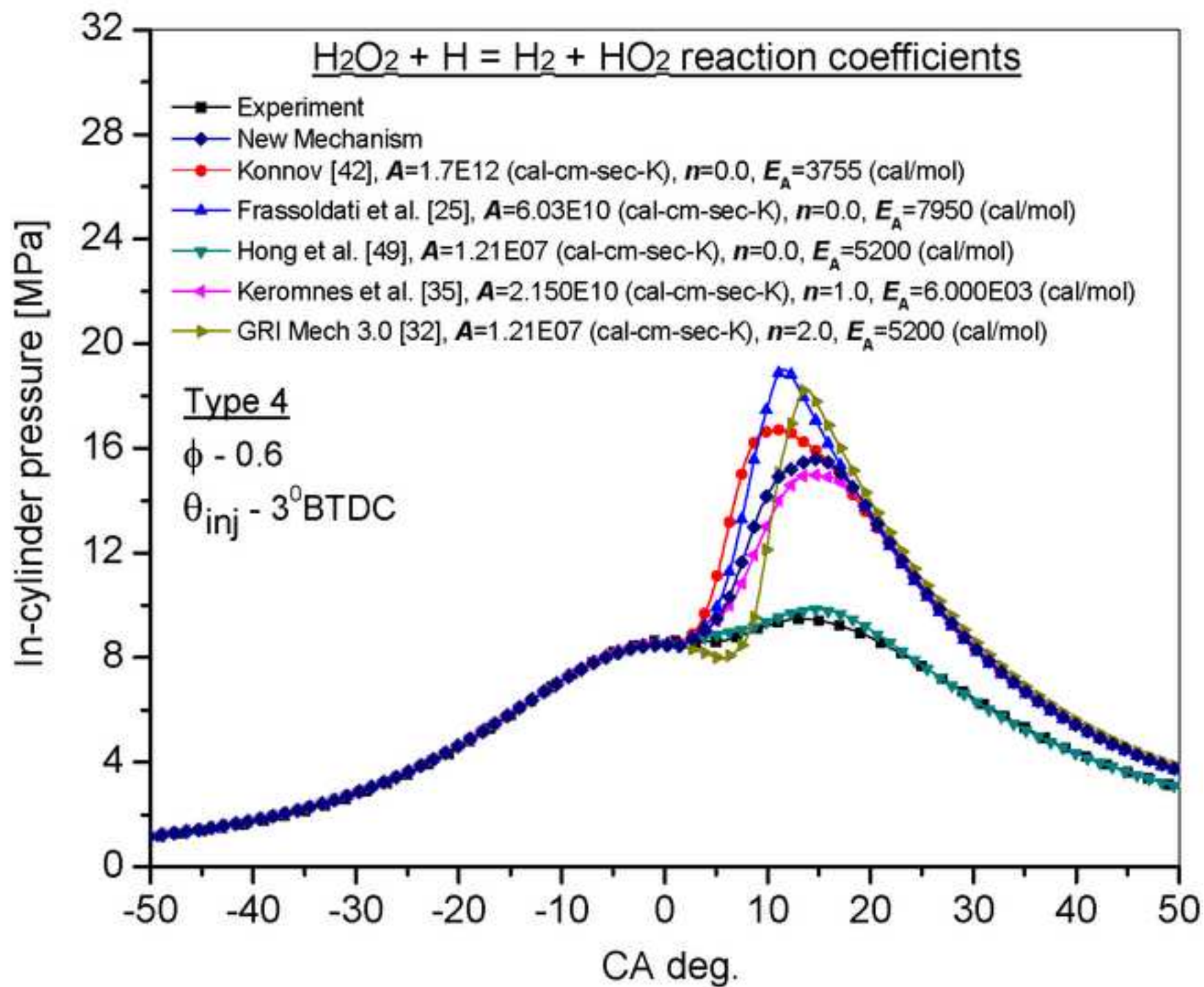
[Click here to download high resolution image](#)

Figure 16

[Click here to download high resolution image](#)

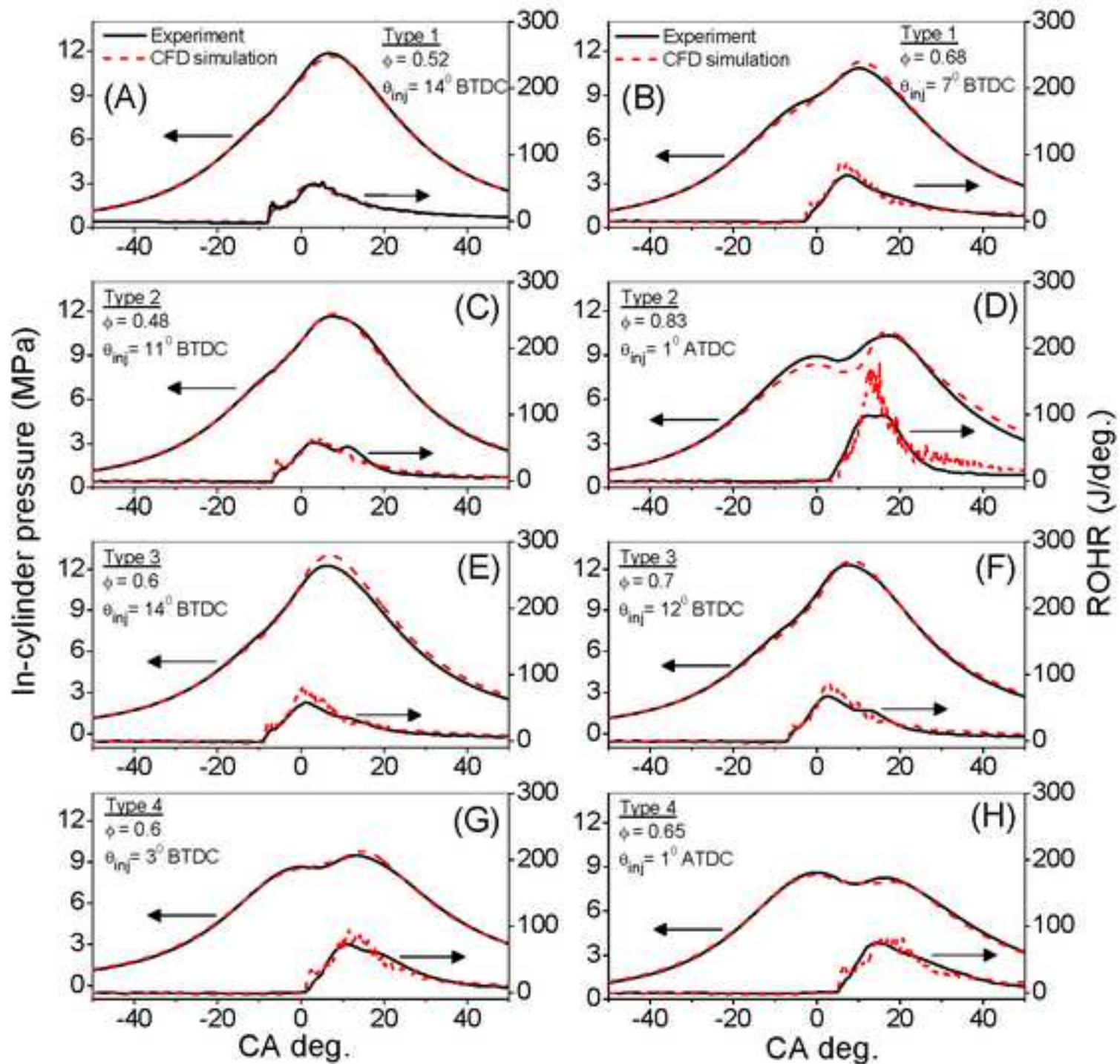
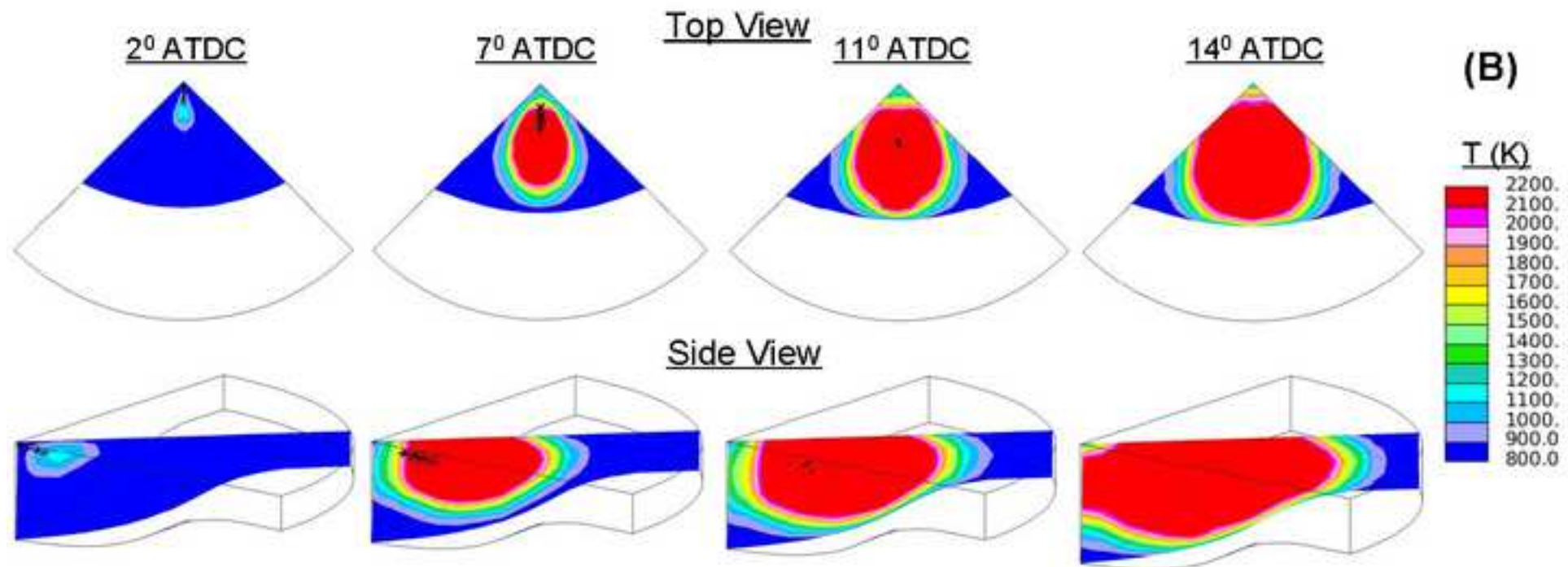
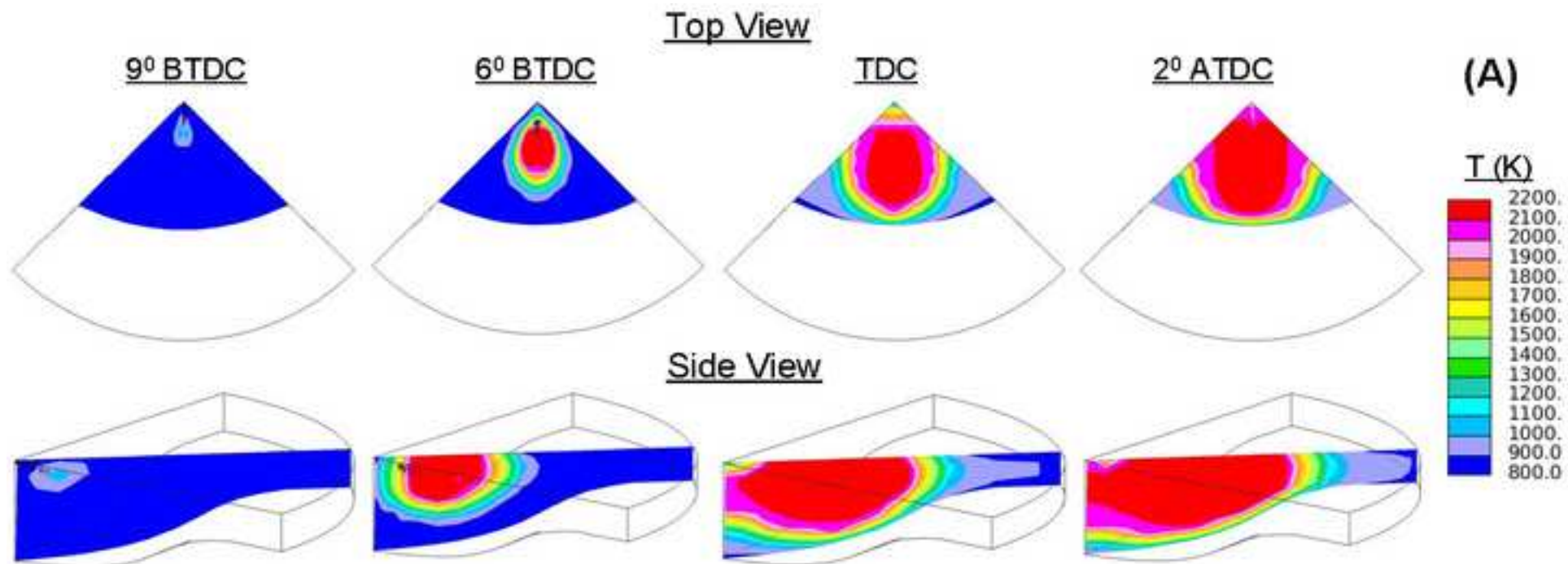


Figure 17
[Click here to download high resolution image](#)



Animation File 1_Top View, Type 3_06

[Click here to download Supplementary Material: Animation File 1_Top View, Type 3_06.gif](#)

Animation File 2_Side View, Type 3_06

[Click here to download Supplementary Material: Animation File 2_Side View, Type 3_06.gif](#)

Animation File 3_Top View, Type 4_06

[Click here to download Supplementary Material: Animation File 3_Top View, Type 4_06.gif](#)

Animation File 4_Side View, Type 4_06

[Click here to download Supplementary Material: Animation File 4_Side View, Type 4_06.gif](#)

Supplementary Material

[Click here to download Supplementary Material: Attachment 1.tif](#)

Supplementary Material

[Click here to download Supplementary Material: Attachment 2.tif](#)

Supplementary Material

[Click here to download Supplementary Material: Attachment 3.tif](#)